UCL Université catholique de Louvain

École polytechnique de Louvain (EPL)

epl

Numerical study of railway track ballast behaviour

Dissertation presented by
Matteo FRANCO

for obtaining the Master's degree in
Civil Engineering

Supervisors
Nicolas DOCQUIER, Paul FISETTE

Readers
Christophe BAYART, Vincent LEGAT

Academic year 2017-2018

Abstract

The railway companies use faster and faster trains and can carry more and more people and goods, increasing maintenance requirements needs due to the increased loads induced by the train. This is due to two main reasons: the rails are welded together and the longitudinal expansion is prevented, causing a buckling that pushes the ballast outwards. In addition, the trainloads apply forces on the sleeper causing it to settle and deform the ballast.

With this thesis, a numerical study of the behaviour of the track ballast is developed so that it can be effectively compared with the results obtained through laboratory tests. For this to happen, it was decided to use the LMGC90 software developed by the Université de Montpellier, which is dedicated to the modelling of granular material, such as the railway ballast.

Although over the years there have been numerous improvements in the elements that make up the track, the ballast has not undergone particular changes. This was modelled using the granular model, the one that best describes the behaviour of the ballast and the resistance to lateral forces and its settlement caused by the application of sinusoidal forces on the sleeper.

In the first part, as for the lateral resistance, simulations have been carried out which have shown the validity of the modelling, according to the different profiles of the ballast bed, its compactness, and the friction coefficients. Moreover, the graph of the lateral resistance as a function of the movements of the sleeper was found to have a consistent behaviour with the tests carried out in the laboratory.

In the second part, graphs were obtained showing the settlement of the sleeper as a function of the stiffness and the number of elastic layers, as well as of the type of force applied to the sleeper. These were compared with curves in the literature, demonstrating the constant presence of three phases in the graphs. Furthermore, the field of accelerations, velocities, and frequencies in the ballast has been studied.

Finally, this thesis mentions possible improvements for future developments.

Riassunto

Le compagnie ferroviarie utilizzano treni sempre più veloci e che possano trasportare un numero di persone e una quantità di merci sempre più elevata, causando problemi di manutenzione dovuti al costante deterioramento dei binari del treno. Questo si deve per due principali motivi: le rotaie sono saldate fra di loro e la dilatazione longitudinale è impedita, causando un buckling che spinge la massicciata verso l'esterno. Inoltre, i carichi del treno applicano delle forze sulla traversina causandone il suo cedimento e la deformazione della massicciata.

Con questa tesi si vuole sviluppare uno studio numerico del comportamento della massicciata del binario, affinché esso sia efficacemente confrontabile con i risultati ottenuti attraverso prove di laboratorio. Affinché ciò avvenga è stato scelto di utilizzare il software LMGC90 sviluppato dall'Université de Montpellier, che sfrutta degli script in Python.

Seppur negli anni vi siano state numerosi miglioramenti negli elementi che compongono il binario, la massicciata non ha subito particolari cambiamenti. Questa è stata modellata utilizzando la modellazone granulare, quella che meglio descrive il comportamento della massicciata e ne sono state studiate la resistenza agli sforzi laterali e il suo cedimento causato dall'applicazione di forze sinusoidali sulla traversina.

Per quanto riguarda la resistenza laterale, sono state eseguite delle simulazioni che hanno dimostrato la validità della modellazione, in funzione dei diversi profili di massicciata, della sua compattezza e dei coefficienti di attrito. Inoltre il grafico della resistenza laterale in funzione degli spostamenti della traversina è risultato avere un comportamento coerente con delle prove effettuate in laboratorio.

Nella seconda parte, sono stati ottenuti delle curve mostranti il cedimento della traversina in funzione della rigidezza e del numero dei sottostrati elastici, nonché del tipo di forza applicata sulla traversina. Queste sono state confrontate con delle curve presenti in letteratura, dimostrando la presenza costante di tre fasi nei grafici. Inoltre si è studiato il campo delle accelerazioni, delle velocità e delle frequenze nella massicciata.

Questa tesi, infine, accenna a dei possibili miglioramenti per degli sviluppi futuri.

Contents

Abstract (English/Italian) **i**

List of figures **vii**

List of tables **xi**

Introduction **1**

Aims . . . 2

Structure . . . 3

1 Railway infrastructure **5**

1.1 Description of the railway infrastructure . . . 5

1.1.1 Rails . . . 6

1.1.2 Rail-sleeper fasteners . . . 7

1.1.3 Sleeper . . . 8

1.1.4 Ballast . . . 9

1.1.5 Subgrade . . . 10

1.1.6 Formation . . . 11

1.2 Applied charges on the railway . . . 11

1.3 Degradation phenomena . . . 12

2 Software and numerical models **15**

2.1 The granular system . . . 15

2.2 The Discrete Element Method . . . 15

2.3 Geometric detection of the contact . . . 16

2.4 Contact laws . . . 17

2.5 Integration schemes and resolution strategy . . . 18

2.6 LMGC90 . . . 18

2.7 Sample modelling . . . 19

2.7.1 Grains . . . 19

2.7.2 Properties of the materials . . . 20

2.8 Bodies contacts definition . . . 20

3 Track's lateral resistance **23**
3.1 Experimental method . . . 23
3.2 Lateral resistance simulation . . . 25
3.3 Creation of the models . . . 25
3.4 Comparison of compactness . . . 28
3.5 Comparison of the lateral resistance . . . 30
3.6 Influence of the mass . . . 37
3.7 Comparison with experimental results . . . 39

4 Vertical settlement **41**
4.1 Experimental models . . . 41
4.2 Implementation of the model in the software . . . 41
4.3 Acceleration analysis . . . 45
4.4 Settlement of the sleeper . . . 47
4.5 Comparison of the compactness . . . 49
4.6 Comparison with a theoretical model . . . 51
4.7 Results for the ballast in the box . . . 53
4.8 Comparison with the experiences . . . 54

Conclusions and perspective **55**
General conclusions . . . 55
Perspectives . . . 56

Bibliography **58**

Appendices **59**

A Profiles of the ballast **61**

B Oscillations of a two mass spring system **63**

C Paraview **67**

List of Figures

1 How the speed and the mass of the trains increased over time 1

1.1 Cross section of a railway track 5
1.2 Division between infrastructure and superstructure 6
1.3 Distribution of the charges, from the wheel to the formation 6
1.4 Flat bottomed (Vignoles) rail is the dominant rail profile in worldwide use 7
1.5 An example of how an extreme heat can cause rails to buckle 7
1.6 Scheme of a free body diagram 9
1.7 First profile of the ballast 10
1.8 Second profile of the ballast 10
1.9 Third profile of the ballast 10
1.10 Scheme of a tamping process 13
1.11 A tamping machine used by Infrabel 14
1.12 Ballast regulator machine 14

2.1 Tasks of a contact resolver 16
2.2 No-penetration laws 17
2.3 Interpenetration law 18
2.4 The difference between a real stone and a modelled stone 19
2.5 Simplified 2D grain modelling for simulation 19
2.6 Deformability of the elastic layer 22

3.1 Cross section of test track during lateral testing with downward load . . . 24
3.2 Test on the lateral resistance of the ballast 24
3.3 First model of lateral resistance: everything is compacted 26
3.4 An example showing how the stones are in the box and how the first profile is created 26
3.5 Second model studying the lateral resistance: compacted zone below the sleeper and not compacted zone beside the sleeper 27
3.6 Third model studying the lateral resistance: compacted zone below the sleeper and beside the sleeper 27
3.7 Fourth model studying the lateral resistance: the compaction is everywhere 28
3.8 Representation of the ballast provided by the Python script 28
3.9 Representation of the ballast provided by Paraview 29

3.10 First model studying the lateral resistance 29
3.11 Second model studying the lateral resistance 30
3.12 Third model studying the lateral resistance 30
3.13 Fourth model studying the lateral resistance 31
3.14 Lateral resistance of a ballast compacted below and beside the sleeper, subjected to a constant displacement 32
3.15 Lateral resistance of a ballast compacted below, subjected to a constant displacement 33
3.16 Lateral resistance of a ballast compacted below the sleeper, subjected to a constant displacement 33
3.17 Lateral resistance of a ballast not compacted beside the sleeper, subjected to an incremental force 34
3.18 Lateral resistance of a ballast not compacted beside the sleeper, subjected to a constant displacement 35
3.19 Lateral resistance of a ballast not compacted beside the sleeper, subjected to a constant displacement 35
3.20 Lateral resistance of a ballast not compacted beside the sleeper, subjected to an incremental force 36
3.21 Lateral resistance of a ballast not compacted beside the sleeper, subjected to an incremental force 36
3.22 Scheme of the mass beside and below the sleeper (red) and beside the sleeper (cyan) 37
3.23 Comparison of the masses of each profile with the total mass of the ballast with the not compacted zone 37
3.24 Comparison of the masses of each profile with the total mass of the ballast where everything is compact. 38
3.25 Velocities of the different bodies in a ballast compacted everywhere 38
3.26 A ballast compacted only below the sleeper after the 10 mm displacement 39

4.1 Numerical model to simulate the settlement of the sleeper 41
4.2 First phase: placement of the stones in the box 43
4.3 Second phase: compaction of the stones in the box 43
4.4 Third phase: hiding of the stones to create the ballast profile 43
4.5 Fourth phase: a vertical force is imposed to the sleeper 44
4.6 Numerical model to simulate the settlement of the sleeper 44
4.7 Force graph with a frequency sweep 45
4.8 Accelerations of the stones in the ballast 46
4.9 Velocities of the stones in the ballast 46
4.10 Acceleration, velocity and settlement of the sleeper pushed by a constant frequency force 47
4.11 Zoom of the vertical settlement of the sleeper pushed by a constant frequency force 48

4.12 Settlements of the sleepers pushed by a constant frequency force, for the cases with no elastic layers, one elastic layer, two elastic layers 48
4.13 Settlements of the sleepers pushed by a frequency sweep force 49
4.14 Compactness of the ballast before applying the force to the sleeper 50
4.15 Compactness of the ballast after applying the force to the sleeper 50
4.16 Movement of the stones in the ballast after applying the force to the sleeper 50
4.17 Compactness of the ballast before applying the force to the sleeper 51
4.18 Compactness of the ballast after applying the force to the sleeper 51
4.19 Movement of the stones in the ballast after applying the force to the sleeper 51
4.20 Scheme of a two mass spring system 52
4.21 Frequency response functions 52
4.22 Acceleration of the sleeper loaded by a frequency sweep 53
4.23 Settlement of a sleeper placed in a box 53
4.24 Vertical settlement of the sleeper as a function of the number of cycles in the experimental model 54

C.1 Velocity of the stones, respectively at $t = 1.000\ s,\ 1.025\ s,\ 1.100\ s$ 67
C.2 Velocity of the stones, respectively at $t = 100.000\ s,\ 100.025\ s,\ 100.100\ s$ 68
C.3 Velocity of the stones, respectively at $t = 199.000\ s,\ 199.925\ s,\ 200.000\ s$ 68

List of Tables

1.1 Classification of the loads 12

2.1 Materials used in the simulations 21

3.1 Summary of the simulations for the lateral resistance 31

Introduction

Context

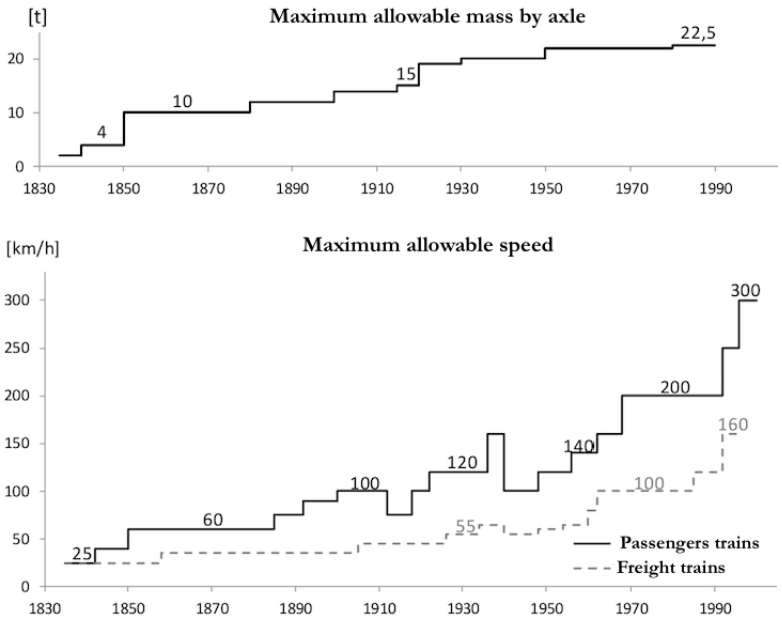

Figure 1 – How the speed and the mass of the trains increased over time (translated [10])

Over the years, the train transport capacity has increased significantly. Trains are getting faster and faster, carrying ever-increasing masses and are required by ever-increasing numbers of travellers. These three factors cause a continuous deterioration of the tracks, which require constant and well-planned maintenance. The tracks, in fact, must be more resistant and maintenance operations must above all consider the problem related to the settlement of the sleepers.

In order to resist these phenomena, the components of the track have become more performing: the sleepers are made of prestressed concrete, with a lifetime that is three times longer than those of the wooden sleepers. The rails use different profiles, such as UIC 60, to withstand greater traffic.

Elastic layers can be placed under the sleeper to better dissipate loads and dampen their effect. Geo-textiles or bituminous layers can be applied to the base of the formation to improve drainage. However, the only component that has not undergone major changes is the ballast, which in fact remains the component that degrades faster. Some railway companies have tried to replace this layer with reinforced concrete slabs, which has a higher initial cost, but a lower maintenance in the long run. Since it is not a component that has been studied for a long time, to date the ballast is the one most used by railway companies.

Aims

The ballast layer must have periodic maintenance, whatever the traffic in circulation, to ensure adequate safety and comfort. The maintenance process most used today is the tamping, an operation similar to what is commonly done with goose down pillows when you want to give a new shape before falling asleep. The difference, obviously, between the two materials is notable because the ballast is composed of irregularly shaped solids with frictions and their displacement must take place in a very short time considering that the tracks on which this operation is to be carried out are long several kilometres.

The tamping is an operation that has existed for over sixty years and its effects have therefore been studied for a long time. Its biggest drawback is that of degrading the components of the ballast: the hammers of the railway tamping machines are inserted between the sleepers and with their high-frequency vibrations they round the stones and break the edges. The degradation is then accelerated and after some operation of tamping, the ballast must be replaced. The study of these operations is very complex and the aim of this thesis is to create a model based on the discrete element method to perform computer simulations that will then be compared with laboratory tests and scientific texts. The thesis is part of the WholeTrack industrial project of the Université Catholique de Louvain, while the software used is LMGC90, developed by the Université de Montpellier. In particular, this thesis is a continuation of the thesis written by Raül Acosta Suñé. I started from his final tips for simulation improvements and I tried to get a more valid model.

The models created use granular modelling and for this type of simulation, they are two-dimensional. With them the lateral resistance of the ballast and the vertical settlements are studied, evaluating how the settlements vary through the use of elastic components. The final aim is to compare the results obtained with experimental results present in the literature or with tests carried out in the laboratory.

Structure

This thesis is divided into four main parts. The first part embraces all the information that allows us to understand how a railway track works, which elements it is composed of and why every element is important. The second part explains what kind of modelling was used to represent the elements of the track, the software and the contact laws that allow starting the simulations. In the third part, there is the study of the lateral resistance of the railway ballast, for each profile and according to the coefficients of friction and compactness. The fourth chapter contains the study of the settlement of the sleeper, connected to the study of accelerations, velocities, and frequencies of the stones in the ballast. Finally, the thesis ends with a summary of the results obtained in this research and some suggestions for the improvement of the simulations already carried out.

1 Railway infrastructure

1.1 Description of the railway infrastructure

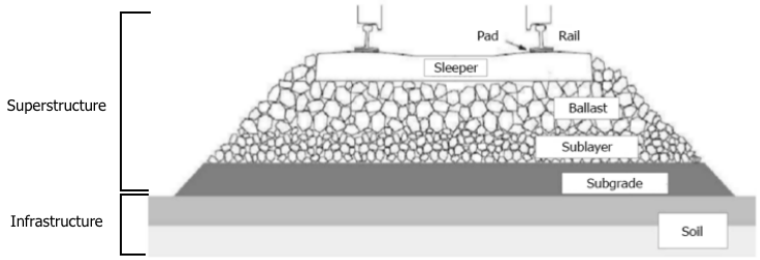

Figure 1.1 – Cross section of a railway track (translated [17])

The term *railway* (or *railway track*) generally refers to the land transport infrastructure, suitable for the movement of trains. It is composed of two parts: the superstructure and the infrastructure (fig. 1.1). The former defines the constructive complex composed of all the elements that should guide and support the train and its wheels. The latter is below these elements and it is in general only composed of the ground, in this case called *formation*.

There are two types of railway lines in Europe: conventional lines and high-speed lines. As defined by the European Union, the latter has been designed to be used by high-speed trains and they include: [17, 13]

- Lines specially built for high-speed trains travelling at speeds generally equal to or greater than 250 km/h;
- Lines specially adapted for high speed, where trains travels for speeds of the order of 200 km/h;
- Specially upgraded high-speed lines, linked to topographic constraints. The optimal speed has to be calculated.

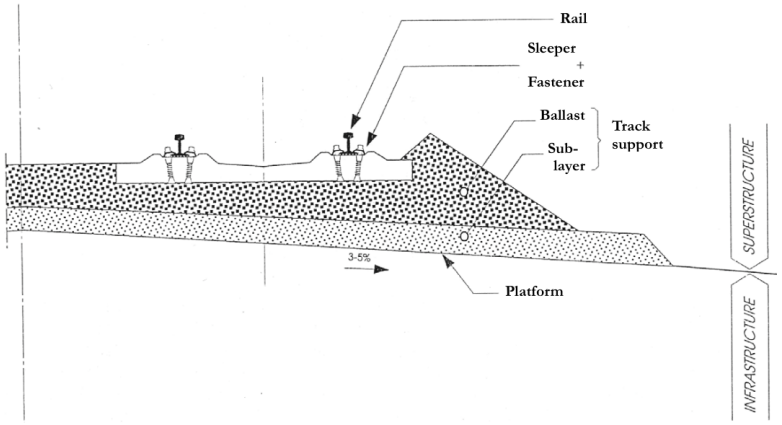

Figure 1.2 – Division between infrastructure and superstructure (translated [15])

The elements of the railway have to bring the train charges from the rails to the formation. The distribution of loads leads to a progressive increase of the distribution area, passing to a reduction of the effort of about 20000 times between the wheel-rail contact points and the formation, [2, 9, 14] in order to reduce the risk that the formation could reach the limit value of the shear strength.

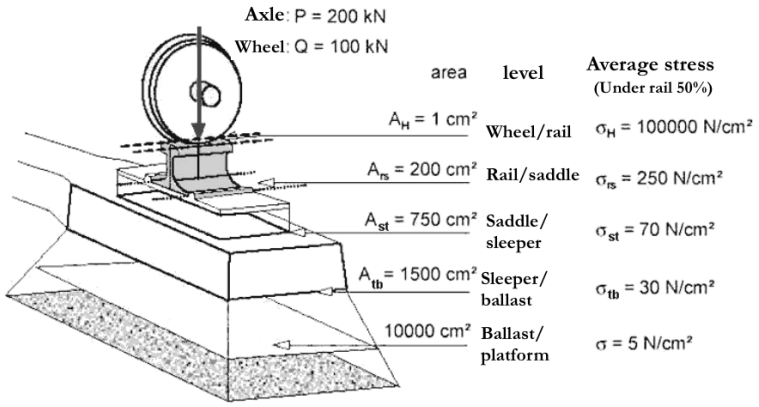

Figure 1.3 – Distribution of the charges, from the wheel to the formation (translated [2])

1.1.1 Rails

Rails are the fundamental element of a track because they are the first element below the trains' wheels and they have to support and guide them. Their section is a double asymmetric T, installed in parallel over a bearing structure called *sleeper*. The most used profile is the one called "Vignoles" (figure 1.4). Its characteristic shape offers a high vertical inertia and an optimal distribution of the shear stresses. Its essential characteristic is its mass per linear meter. The UIC, the worldwide rail organisation, has standardised two profiles: 54 or 60 kg per linear meter, in rolled steel.

The track gauge is the distance between the two tangents of the internal borders of the railhead and it is not universal: different countries and rail systems can have different gauges. In Italy and Belgium, the gauge of the entire network is 1435 mm, defined internationally as Standard Gauge or Standard, derived from the gauge of George Stephenson to present the world's first locomotive to the world.

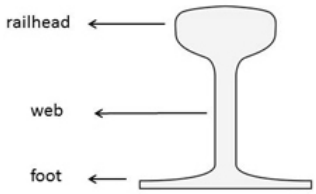

Figure 1.4 – Flat bottomed (Vignoles) rail is the dominant rail profile in worldwide use [23]

The rail profile is composed of three parts:

- The upper part called *railhead*, and it is the part in contact with the wheels;
- The *foot*, the base of the rail that is in contact with the sleeper
- The *web*, that links the other two parts.

The length of the rails is 36 or 72 metres. Each profile is welded, and because of the this, there could be some buckling effects (fig. 1.5) that could laterally move the rails against the ballast.

Figure 1.5 – An example of how an extreme heat can cause rails to buckle [6]

1.1.2 Rail-sleeper fasteners

The connection between the rail and the sleeper has undergone various changes over the years. For the Vignoles rail, stability is facilitated thanks to the wide and thin base of the foot. Originally, to fix the rail, a wooden wedge was used for a rail with a double railhead

and when the part in contact with the wheels was worn, the rail could be rotated to use the non-worn part. Today the fastening system is mechanised to ensure good elasticity and faster times. Fastening is done with mechanical machines that automatically connect the sleeper and the rail.

It is also important to place elastic rubber layers under the sleeper to dampen vibrations caused by passing trains.

1.1.3 Sleeper

The sleeper is an element that has the role of transmitting train loads from the rail to the ballast, ensuring a constant track gauge and inclination between the rails. [17]

The two most commonly used materials for the sleeper are wood, almost exclusively used years ago, and concrete, which makes the sleeper heavier, improving stability, noise isolation and giving the track a longer life. In some areas of Italy, wooden sleepers are preferred to those in concrete because environmental conditions such as the heat and salt carried by the sea can corrode the armature of the sleeper.

There are two types of concrete sleepers:

- Monoblock: sleepers made of a single piece of concrete. They are characterised by a good stability and they could last around 50 years;
- Bi-block: sleepers composed of two concrete parts connected by a metal bar. Their advantage is the reducing damage from torsional forces on the sleeper centre due the more flexible steel connections. They cost less but they last less (30-40 years) because of the possible corrosion of the metal bar.

The lateral anchoring of the sleeper in the ballast is very important for the lateral stability of the track. It could help to reduce the buckling effect of a welded rail subjected to heat dilatation.

The sleepers have been made increasingly heavy and stable as a result of the invention of reinforced concrete, but the disadvantage is in the low vibration damping capacity.

Weight is an important element. The greater the weight of the sleeper, the greater the force to be applied to move this sleeper.

$$\begin{cases} F \leq \mu \cdot m \cdot g \\ T \leq \mu \cdot N \end{cases} \tag{1.1}$$

Where:

- F is the applied force;

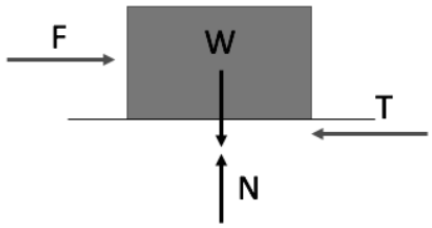

Figure 1.6 – Scheme of a free body diagram

- T is the friction force;
- μ is the friction coefficient;
- N is the normal force;
- g is the gravity acceleration.

1.1.4 Ballast

The main purpose of the ballast is to ensure a solid and stable support base for heavy structures that must rest directly on the ground. Soils are often unsuitable to directly support the structures because they can be wet, yielding and rich in vegetation and particularly they can undergo considerable changes as a result of floods, winds etc.

The ballast, thanks to its composition of small and medium-size stones, protects the structure from humidity and lets the water pass underneath, so that it can subsequently evaporate.

The crushed stone is regulated by EN 13450:2003 norm which defines mechanical and physical properties. For Italian standards, the gravel is considered suitable if its density is higher than 2550 kg/m^3. The particle size fraction, comprised between two sieves of dimensions 31.5 and 50.0 mm, must have a number of stones equal or greater than 50%. [18]

The ballast is not only the base of the train tracks but it also anchors the sleeper reducing the longitudinal and transversal effects.

In Belgium, Infrabel has defined three profiles of ballast to be used for its tracks. [3, 17]

1. The first profile (fig. 1.7) has a small protuberance of 0.10 m. It is used for speed:
   - $v < 200\ km/h$ and $v \geq 40\ km/h$;
   - $v > 200\ km/h$ and the presence of particular elements on the track, such as expansion devices;
2. The second profile (fig. 1.8) is the one used on the high-speed line, i.e. for train speeds above 200 km/h and it does not have the protuberance of 10 centimetres to

avoid the risk of flying stones;

3. The third profile (fig. 1.9) is used for low speeds, for example for the accessories tracks.

Obviously the first profile has a greater lateral resistance compared to the third profile, because it has a greater number of stones and therefore a greater mass on the side of the sleeper. The sleeper finds a greater difficulty in moving the ballast.

The figures 1.7, 1.8, 1.9 provided by the Infrabel track design studio show the three ballast profiles. [3]

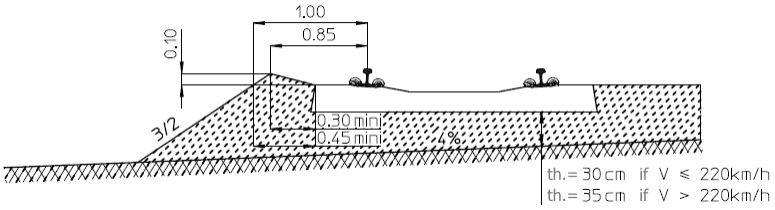

Figure 1.7 – First profile of the ballast (translated [3])

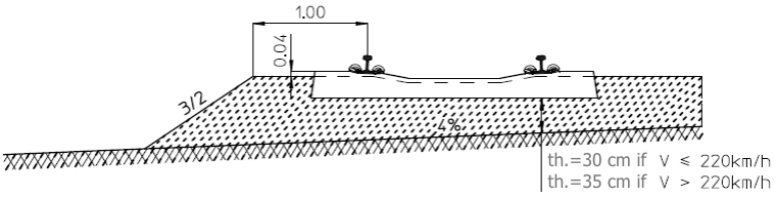

Figure 1.8 – Second profile of the ballast (translated [3])

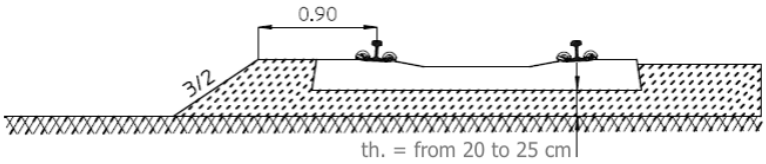

Figure 1.9 – Third profile of the ballast (translated [3])

1.1.5 Subgrade

In transport engineering, subgrade is the native material underneath a constructed road, pavement or railway track. [22] The aim of this layer is to avoid the reaching of the shear strength in the formation. It also improves the protection against the frost and it improves the draining.

The subgrade is generally composed of gravels with a size of $20-40\,\text{mm}$. In order to improve the lifespan it is possible to add a bituminous concrete or a geotextile. [14]

1.1.6 Formation

The formation constitutes the infrastructure of the track and can be built with an embankment or it can be a bridge or a tunnel. Its most important feature is the weight capacity: the formation is the last element that makes up the track, takes the remaining loads and influences the long-term behaviour of the sustained superstructure.

Another important aspect is the stiffness, which in some cases can help to decrease the settlement of the tracks. For this reason, recent research studies the settlement of the tracks analysing the use of elastic layers placed on the formation.

1.2 Applied charges on the railway

The stresses to be taken into account during train transit are as follows: [24]

- Lengthways in the wagon:
  - Up to four times the mass of the load for goods that are rigidly secured;
  - Up to once the mass of the load for goods that can slide lengthways in the wagon;

  They are mainly due to train's acceleration and deceleration and temperature variations, especially for welded bars. They are generally negligible compared to vertical and horizontal efforts;
- Crosswise in the wagon up to 0.5 times the mass of the load. They are caused by the centrifugal effect when cornering and by forces of thermal origin due to welding of the tracks. They should not be underestimate in order to prevent the buckling phenomenon. In fact, the ballast is less rigid in the lateral direction;
- Vertically up to 0.3 times the mass of the load, which encourages the displacement of the goods. They are divided into static loads, such as the mass of the train, and dynamic loads, due to the interaction between vehicle and track.

The UIC classifies the line types based on the load. The lines of each railway are classified into categories per the permissible mass per axle and mass per linear metre, as shown in table 1.1.

The load limits are marked on the wagon and it is that one from the lowest line category on the route in question. This limit must not be exceeded. [24]

Table 1.1 – Classification of the loads. [24]

Line category	Maximum mass per axle	Maximum mass per linear metre
A	16.0 t	5.0 t/m
B1	18.0 t	5.0 t/m
B2	18.0 t	6.4 t/m
C2	20.0 t	6.4 t/m
C3	20.0 t	7.2 t/m
C4	20.0 t	8.0 t/m
D2	22.5 t	6.4 t/m
D3	22.5 t	7.2 t/m
D4	22.5 t	8.0 t/m
E4	25.0 t	8.0 t/m
E5	25.0 t	8.8 t/m

1.3 Degradation phenomena

The train loads induce a slow degradation of the track, both in terms of geometry and the state of the materials. For this reason it is necessary to carefully design the line by choosing the appropriate materials.

The type of train and the type of rolling material circulating on the track can influence the degradation status of the track. A regional train, for example, travels much slower than a high-speed train, with much less important dynamic loads. If there are any imperfections in the contact between the train wheel and the rail, dynamic overload effects occur, implying a faster degradation.

Atmospheric phenomena must also be considered during track design. For example, in some Italian lines, RFI, the owner of Italy's railway network, has decided to apply a white paint over the rails, in order to decrease the value of the thermal expansion coefficient, thus decreasing the dilatation efforts.

There most important maintenance process is called *tamping* and it is used when the rails no longer satisfy the tolerance thresholds. The machine takes a measure in the first phase where it detects everything in terms of trajectory, levelling and inclination. A track in comparison to the other must be flat without any inclination. If there is an error of 3-5 millimetres, this must be zero. Information are transmitted to the system and the rail will be straightened or re-aligned. The machine vibrates at high frequency to compress the ballast under the sleepers and the track remains in its new position.

The hammers break the stones and smooth the edges. Breaking the stones means reducing the compaction of the ballast and therefore also decreasing its lateral resistance also

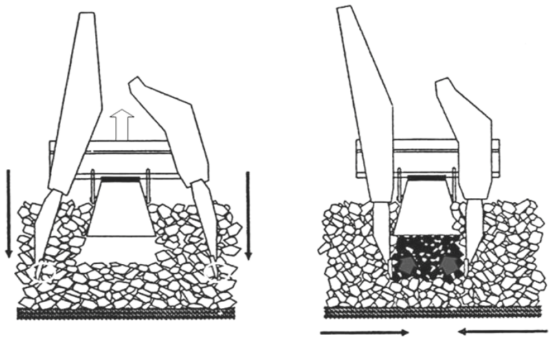

Figure 1.10 – Scheme of a tamping process [20]

because only the zone below the sleeper is compacted and not on the sides, which will then need to be especially studied in the curves of the tracks. [17, 14]

Approximately, a tamping is effective for 40-50 million tons of passage, or more or less 4-5 years of traffic, depending on the the number of tampings realised. [14]

Generally, this operation can be accompanied by the use of another machine: a ballast regulator, also known as a *sweeper*, that is used to shape the different ballast profiles and to compact these profiles pushing from the top of the protuberance (figure 1.12).

(a) *View of the hammers from the platform*

(b) *Internal view of the tamping machine*

Figure 1.11 – A tamping machine used by Infrabel

Figure 1.12 – Ballast regulator machine [21]

2 Software and numerical models

2.1 The granular system

A granular material is a conglomeration of discrete solid, macroscopic particles characterised by a loss of energy whenever the particles interact and they are not chemically linked. They are use in different fields, from agriculture to pharmacy industry. [1]

The behaviour of a solid material divided into very small grains is different from the behaviour of its material in the solid, liquid or gas state and depends on the applied energy, which is dissipated very rapidly.

The granular materials are difficult to study because there are complex limit conditions and many contacts laws. A granular system is stable if low-stress increases induce small deformations, therefore the modelling of quasi-static behaviour assumes that these increments have a finite value and that the fluctuations of these values can be neglected. [16] In addition, the friction forces should be calculated because they are the stabilising elements and they can't be neglected. The calculation of these forces makes the process longer.

Thanks to the properties of the granular systems, the stability of the track is also analysed through numerical simulations.

2.2 The Discrete Element Method

The principle of the discrete element method (DEM) is to integrate the motion equations by analysing the interactions of the particles by contact or friction. In general, on one step $[t,\ t+h[$, three main phases can be identified: [11]

- Contact detection;
- The resolution of contact forces: the speeds and/or rotations that each particle will

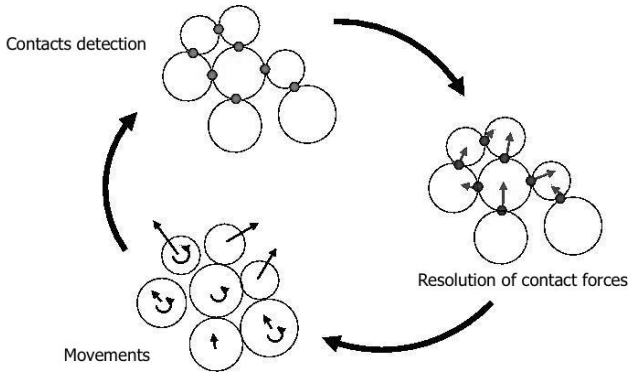

Figure 2.1 – Tasks of a contact resolver (translated [11])

undergo are calculated;
- The movement of each particle.

Today the two most used approaches are the following:

- The regular approach, or Smooth: the relative displacements between two particles at the contact point or the interpenetration are used in correlation with a law which regulates the contact force;
- The non-regular, or Non-Smooth approach: it considers the contact and friction interactions, using the laws of motion and the dissipation equation.

The NSCD (Non-Smooth Contacts Dynamics) doesn't allow the overlapping of two particles and it considers the perfect rigidity of contacts. Trough the Signorini-Coulomb law is possible to determine the speed and the force of each stone, avoiding the penetrations. This method is commonly used because it allows different shapes, convex and concave, with bigger time steps.

2.3 Geometric detection of the contact

The contacts can have different types of polyhedral particles such as the ballast. These contacts can be represented by a point, a line or a surface.

In the LMGC90 software, the contacts between two bodies always have a candidate body A and an antagonist body B. The aim of the software is to make the contact happen but A does not have to penetrate the body B. Both have a local reference point and the direction between these two points must be considered. [16] Through the distance between these two points, the distance between the two bodies is calculated and whether or not the overlap occurred. As a first step, an alert distance is established, which consists in estimating the proximity of two stones and if this distance is sufficiently high, other bodies are analysed.

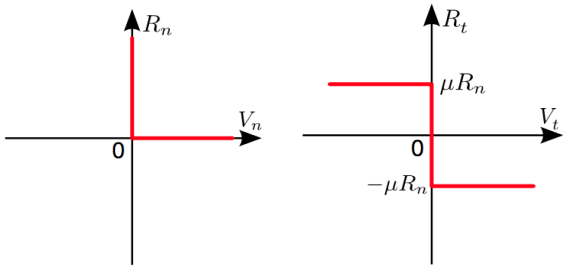

(a) *No-penetration law* (b) *Fiction law*

Figure 2.2 – No-penetration laws [17]

The problem of this type of simulation is the large number of cycles, and therefore of time, to be performed. If, as in the case in question, there are many bodies, it is necessary to calculate the contact that occurs in a certain step between all the bodies in question. [16] In this thesis, only two-dimensional bodies were used.

2.4 Contact laws

To study the behaviour of the ballast, the choice of the contact law is fundamental, because it regulates the contacts between the grains and therefore their positions. It was chosen to use the Signorini-Coulomb law, with the following constraints:

$$\text{if } g \leq 0 \;\Rightarrow\; \begin{cases} R_n \geq 0;\; V_n \geq 0 \\ V_n \cdot R_n = 0 \end{cases} \tag{2.1}$$

Where:

- g is the gap between the two particles. If this space is null it means that a contact reaction is present;
- R_n is the normal reaction of the particle;
- V_n is the relative normal speed of the particle.

However, the space g is always positive because there is no grain penetration. The only case where there could be the interpenetration is with the analysis of the vertical settlement, where a interpenetration is needed to study the elasticity of some elastic bodies. The law is shown in figure 2.3

$$\text{if } g \leq 0 \;\Rightarrow\; R_n = -k_n \cdot g \tag{2.2}$$

Where k_n is the stiffness.

With regard to the friction law that should regulate the frictional contact between the

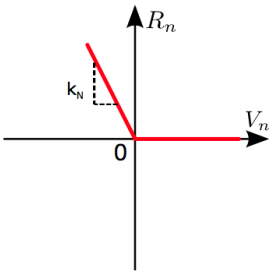

Figure 2.3 – Interpenetration law [17]

bodies, the Coulomb law was used:

$$\begin{cases} \|dR_t\| \leq \mu \cdot dR_n, & \text{if } V_t = 0 \\ dR_t = -\mu \cdot \frac{dR_n}{\|dR_n\|}, & \text{if } V_t \neq 0 \end{cases} \tag{2.3}$$

Where:

- R_t is the tangential reaction of the particle;
- R_n is the normal reaction of the particle;
- V_t is the tangential speed;
- μ is the friction coefficient.

The two bodies move only if the tangential force exceeds the value $\mu \cdot R_n$.

2.5 Integration schemes and resolution strategy

The goal of time integration schemes is to discretise the movement of a particle when there are some contacts, in order to have a better precision.

Two approaches are possible: [16]

- Trough the *event-driven* method: the time is not uniformly divided, but the interval is adapted in such a way that the collision moment falls in this time step. It is not used in this thesis because there would be an high number of contacts and it would require an high number of interactions;
- Trough the *time-stepping*: the time is divided into many steps of equal duration. It is implemented in LMGC90 and it is used in this thesis.

2.6 LMGC90

The software used during the simulations is LMGC90. The LMGC90 is a multipurpose software developed in the Université de Montpellier, in France, capable of modelling a

(a) *The real shape of a stone placed in the ballast*

(b) *How the stones are seen by LMGC90* [19]

Figure 2.4 – The difference between a real stone and a modelled stone

collection of deformable or non-deformable interacting through simple interaction (friction, cohesion, ...) or complex multi-physics coupling (fluid, thermal, ...). [11]

LMGC90 can use bodies with different shapes, from polygons to spheres, in two or three dimensions.

In this thesis, only irregular polygons where used to model the stones placed in the ballast, and, in addiction, rectangular elements such as walls, sleeper, formation and elastic layers.

2.7 Sample modelling

2.7.1 Grains

(a) *Real shape* (b) *Real shape vs modelled shape* (c) *Modelled shape*

Figure 2.5 – Simplified 2D grain modelling for simulation [17]

The most difficult track's component to model is the ballast: in fact, it is necessary to define the shape of each stone and then place the sleeper on it. The ballast must try to look as much as possible to an existing ballast, that is, with the area compacted under the

sleeper and a less compact area on the sides. It is also important so have some different shape for the stones because a model with only one shape will not be enough accurate.

Also appropriate friction coefficients and appropriate interaction laws must be provided. Moreover, due to the great number of calculations to be performed through the computer, it was decided to use 2D models, giving a prismatic shape to all the components of the model, with a depth of one meter for each body (figure 2.4).

The shape of the stones used for the simulations was obtained from the stones that the Sagex company supplied to the WholeTrack group. Through a video-granulometry process, different shapes were taken, obtaining a polygonal line and then simplified to obtain a convex shape (fig. 2.5) [17]. The Non-Smooth Conctacts Dynamics method can consider concave shapes but it would take more time, it would be more difficult to resolve the contact and it requires a specific algorithm for the contact detection.

2.7.2 Properties of the materials

It would be impossible to run a simulation with the discrete element method if, in addition to the shape, a material with its mechanical properties was not assigned. It is necessary to specify that the bodies are considered rigid, that is with an elastic modulus tending to infinity, [17, 11] except for the elastic layer placed below the sleeper and above the formation.

Through the first simulation model, the lateral resistance of the ballast is studied and therefore it is necessary to insert the properties of the stones, the sleeper, the formation and some artificial walls that help to realise the compaction. For the second model, that studies the vertical settlement of the sleeper, an elastic layer is added. The assigned material is the caoutchouc, a material commonly used in the construction of the railway tracks because it helps to reduce the acoustic and mechanical vibrations, with a density of $930\,\mathrm{kg/m^3}$.

2.8 Bodies contacts definition

For the properties of granular materials, the definition of friction coefficients is a very important aspect because it affects the behaviour of the structure.

Maynar Melis calculated a friction coefficient between the grains that falls in a range that goes from 0.577 to 0.839. Different coefficients were used, in order to evaluate the changes in the results of the simulation and to study the different behaviours. [17, 12]

For the case of the friction between the grains, only 0.7 and 0.8 were used, in order to be in that range. The contact of the grains with the formation is equal to 1, because, in

Table 2.1 – Materials used in the simulations

Simulation that study the lateral resistance			
Element	Material	Density (kg/m^3)	Type
Stone	Porphiry	2800	Rigid
Sleeper	Concrete	2500	Rigid
Wall	Concrete	2500	Rigid
Simulation that study the settlement			
Stone	Porphiry	2800	Rigid
Sleeper	Concrete	2500	Rigid
Wall	Concrete	2500	Rigid
Elastic layer	Caoutchouc	930	Elastic

reality, the stones meet a wrinkled soil and there is more adherence.

For the contact between the grains and the sleeper, 0.5 and 0.7 as friction coefficients were used to check if the lateral resistance of the ballast profiles increases as in the reality.

For the second model that studies the vertical settlement, there could be two elastic layers.

In addition to the contacts explained above, two other laws are added: [11]

- ELASTIC_ROD: the law used for the elastic layer places below the sleeper. It adds a spring rod to some specified points and its importance it is in the fact that the layer doesn't fall because of the gravity, but it is glued to the sleeper. The reaction force is proportional to the deformation;
- ELASTIC_REPELL_CLB: it describes a normal reaction force proportional to the gap, otherwise the reaction force vanishes when the contactors separate. The friction law is Coulomb's law and it is useful when there are physical reasons to take elasticity into consideration.

The elastic layers have one degree of freedom and their behaviour is shown in the figure 2.6.

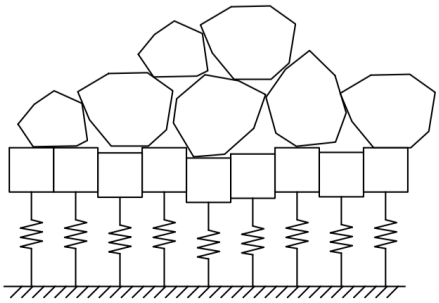

Figure 2.6 – Deformability of the elastic layer

3 Track's lateral resistance

3.1 Experimental method

As already mentioned in section 1.1.1, in addition to the longitudinal and vertical loads, it is important to study the influence of lateral loads on the resistance of the ballast. If before this study was not necessary, today it is essential because of the increase in the number of passengers and the number of goods transported.

The TU Delft Roads and Railways Research Laboratory conducted a series of full-scale three-dimensional ballast resistance tests using a rail track panel. For our objectives, only the results of the tests regarding the lateral resistance are compared with the results obtained in this thesis. [25]

The components that make up the instrumentation used to perform the test, shown in figure 3.1, are: [25]

- Two rail pieces, UIC 54 section;
- Five NS90 concrete sleepers;
- Ballast bed of crushed stone 30/63, a thickness under sleeper of 30 cm;
- Ballast mat, James Walker type (FC600/FC101);
- Concrete slabs (Stelcon): 2 m × 2 m × 10 cm, total 120 m^2;
- Sand foundation (subgrade).

The load introduction in the lateral direction is achieved through two diagonal rods connecting the hydraulic actuator, to the track section with a force of 150 kN. Two connecting beams are welded between the rails to reinforce the track panel enabling a more uniform load introduction. The actuators are programmed under displacement control to fulfil a complete measurement with a constant low velocity of 10 mm/min. [25]

All measurements in the test were automatically and digitally recorded and imported into the Matlab environment, where the research team has obtained an automatic curve

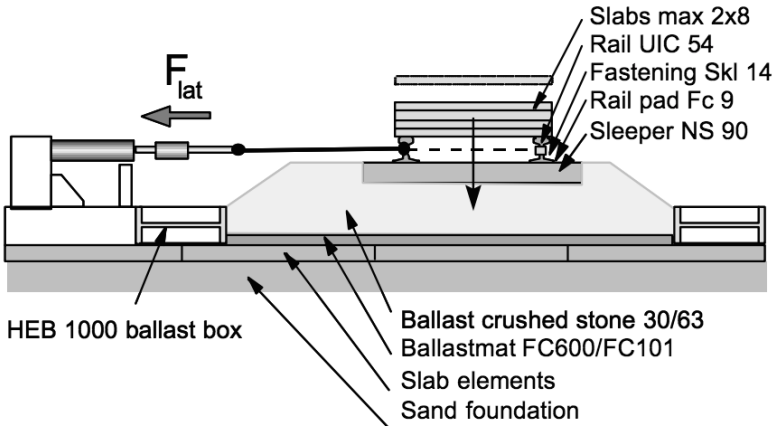

Figure 3.1 – Cross section of test track during lateral testing with downward load [25]

fitting routine, in order to produce the best fit of the data based on the formula:

$$F = a_1 \cdot x \cdot e^{-b_1 \cdot x} + a_2 \cdot (1 - e^{-b_2 \cdot x}) \tag{3.1}$$

Where:

- F is the lateral force;
- x is the lateral displacement;
- a_1 and a_2 are two linear curve-fit parameters;
- b_1 and b_2 are two nonlinear curve-fit parameters.

Equation (3.1) is a mathematical approximation and does not claim any physical meaning.

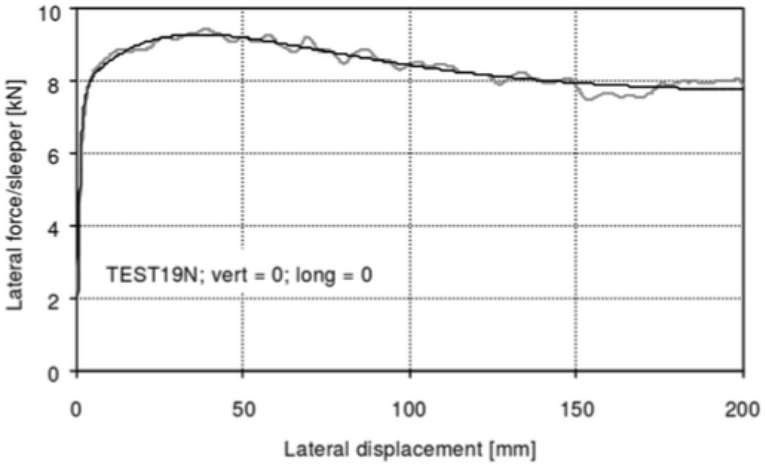

Figure 3.2 – Test on the lateral resistance of the ballast [25]

Figure 3.2 shows one graphical result for the lateral resistance without both longitudinal and vertical load and its curve-fit approximation. It is possible to observe that there are

three main parts: [25, 17]

- A phase where the displacements are very small compared to the lateral forces;
- A logarithmic phase that ends with an inflection point;
- An asymptotic line that reaches a lateral resistance value.

3.2 Lateral resistance simulation

The results of lateral resistance of the track mentioned above are compared with some numerical simulations carried out with LMGC90. Although in reality the physical model to move a sleeper is very complex, in simulations it is very simple: a force or a speed is directly imposed on the sleeper. The simulations are carried out for four different profiles, in order to compare them and to evaluate the different lateral resistance and, in general, a simulation stops when the sleeper is displaced for 10 mm.

The force imposed is an increasing horizontal force, and for each time step it is possible to store the reactions of the sleeper (or other selected bodies) and a plot studying the correlation between the force and the displacement is the final output.

The increasing horizontal forces are:

- $\Delta F = 1.0\ N$ each time step, that is every millisecond;
- $\Delta F = 1.5\ N/ms$;
- $\Delta F = 2.0\ N/ms$.

When a force is imposed, probably there is a kinetic absorption on the grains of the ballast and in the graphs there is not the first linear phase mentioned in section 3.1. In order to better understand this phenomenon, an imposed constant velocity was applied to the sleeper, with a value of $v_x = 2\ mm/s$.

In addition, it was decided to evaluate the lateral resistance in the different sides of the sleeper, with the respective percentages, to better understand the influence of the compaction. Below the sleeper, where there is a compacted zone, the forces should be more influential than the forces in a not compacted zone.

3.3 Creation of the models

In the first simulation of the lateral resistance (figure 3.3), half-track is modelled. It has been chosen to have a very compact ballast, both below the sleeper and on its sides, which generally does not represent reality. In order for this to happen, numerous stones have been placed in a large box representing the ballast in a railway track. All these stones have been dropped due to gravity and once they are stable, a vertical wall on the right

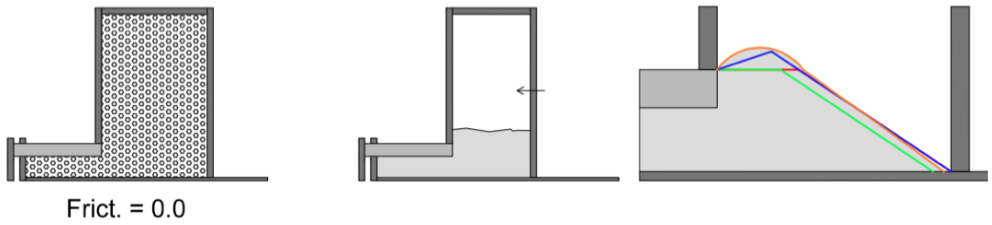

Figure 3.3 – First model of lateral resistance: everything is compact

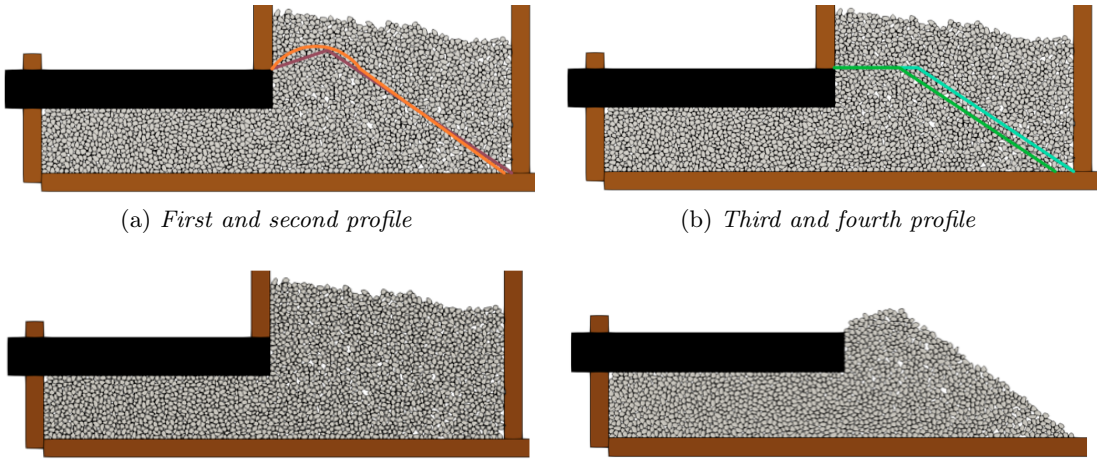

(a) *First and second profile*

(b) *Third and fourth profile*

(c) *Modelled view of the grains in the box*

(d) *Shape of the ballast using the first profile*

Figure 3.4 – An example showing how the stones are in the box and how the first profile is created

has the task of pressing these stones to compact them. The force exerted by this wall is of constant type, in fact, the wall is displaced with a constant speed equal to 1 m/s.

The next step is the creation of ballast profiles provided by Infrabel. This means that the superfluous stones that do not fall into these four profiles have to be hidden. The equations are in the appendix A.

Another model realised (figure 3.5) is a model that should reflect the conditions of the tamping phase. When this maintenance operation takes place, the pistons enter the part of the ballast placed between two sleepers and through strong vibrations they begin to move the stones. It is easily conceivable that in the part below the sleeper there will be a very contact zone, while in the part on the side of the ballast there will be a not very compact area. To make this situation, the stones are placed in a large container and are dropped due to gravity. Once they are stationary and stabilised, the right vertical wall is pushed against them with a constant speed of 1 m/s. Also, in this case, the friction between the stones is null to speed compaction and to simulate the fluid behaviour of the bodies during the tamping phase. Once this phase is over, the friction is correctly reset and the stones on the side of the sleeper, i.e. those where a non-compact part is

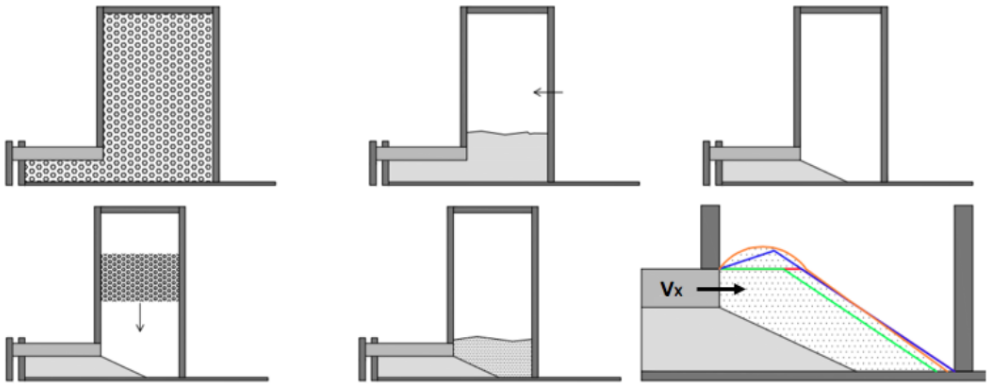

Figure 3.5 – Second model studying the lateral resistance: compacted zone below the sleeper and not compacted zone beside the sleeper

expected, are hidden. Later, other grains are put back into the container and dropped due to gravity. The wall no longer pushes the grains, leaving them in their stabilised position and many more empty between them. Figure 3.5 shows the compact area, below the sleeper, and the non-compact area on its side.

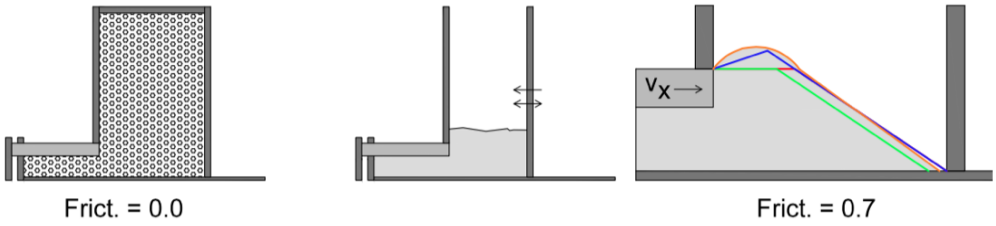

Figure 3.6 – Third model studying the lateral resistance: compacted zone below the sleeper and beside the sleeper

Figure 3.6 shows another compaction that is very similar to that of belonging to first model (fig. 3.3). In this case, at one-third of the simulation, the right vertical wall pushes the stones through a sinusoidal movement with the following equation:

$$v_x = A \cdot \sin(2 \cdot \pi \cdot f \cdot t) \tag{3.2}$$

Where:

- A is the amplitude: 0.2512 ;
- f is the frequency: 40 Hz;
- t is the time.

In this way, the grains are pushed to the left with a less abrupt but still effective movement.

In this model, as for the first and the third model, there is a compaction in every zone of the ballast. The horizontal upper wall falls due to gravity and it is pushed against the

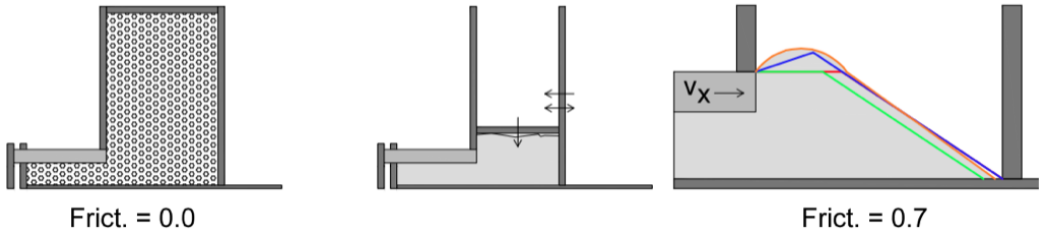

Figure 3.7 – Fourth model studying the lateral resistance: the compaction is everywhere

track stones. At one-third of the simulation, the software adds an incremental force of 500 N and the simulation stops until it reaches 50 kN. In addition to this, like the previous model, the right vertical wall tries to compact the stones with a sinusoidal movement (figure 3.7).

3.4 Comparison of compactness

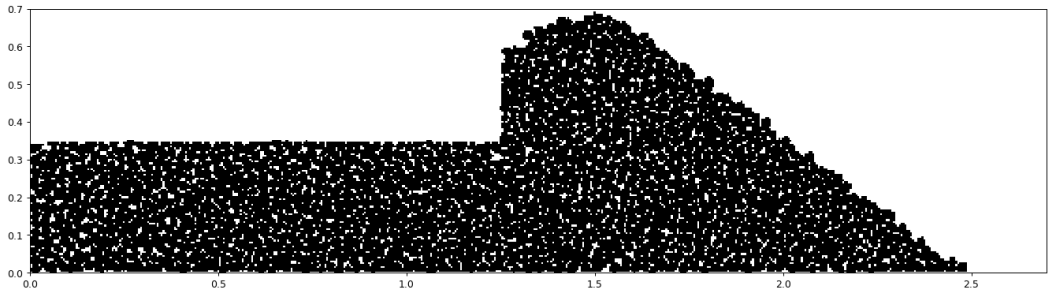

Figure 3.8 – Representation of the ballast provided by the Python script. The unit of measure is the meter

For all the simulations carried out, the compactness of the ballast on the side and below the sleeper was studied with the aim of analysing the variation of compaction during this model creation process. The compaction of the ballast has been studied in three different phases with the use of Python scripts. Figure 3.8 is the graphic result of a script that checks for each point of the ballast whether there is a stone or not: if it is, it draws a little black square, otherwise a small white square. For reasons related to the complexity of the calculation, it was decided to use a 5 mm step, so that the result is fairly reliable. In fact, there is not a big difference with the image provided by the LMGC90 software (figure 3.9).

Then, it was chosen to represent squares of size 45 mm × 45 mm, so that each square contains a value that is the mean of a square containing 9 × 9 points. For each cell a colour was identified representing the percentage of points, i.e. the percentage of space covered by one or more in that square. The dark blue indicates that the area is very compact, while the dark red indicates that there is a gap in the ballast.

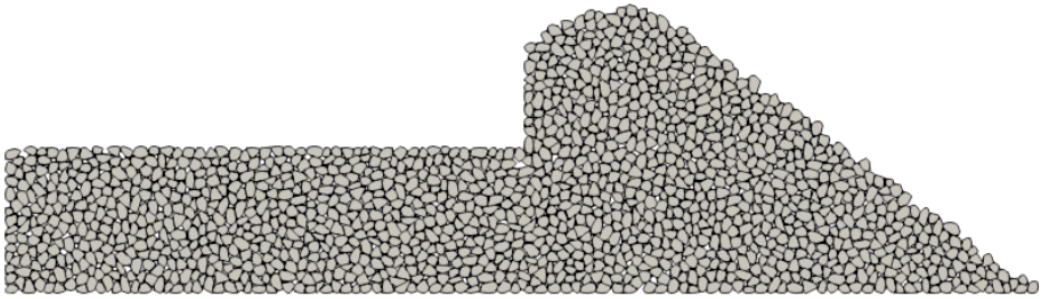

Figure 3.9 – Representation of the ballast provided by Paraview

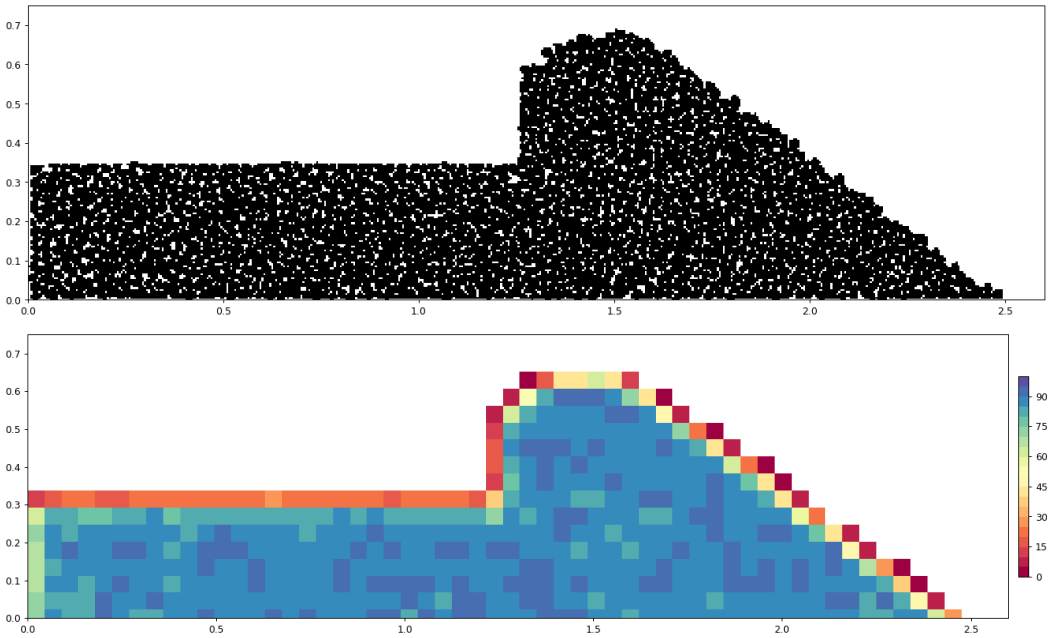

Figure 3.10 – First model studying the lateral resistance. The unit of measure is the meter

The figures 3.3 and 3.5 show two opposite cases: the ballast with a compaction carried out everywhere and the ballast which has not undergone a compaction on the side of the sleeper. As expected, there is an obvious difference in compaction in the latter area, so the script used is valid.

The fourth model (fig. 3.7) has a greater compaction than the third (fig. 3.6) because in addition there is the presence of a wall that pushes from the top towards the bass. It can be said, however, that the compaction is not so evident, probably due to the fact that the simulation was not carried out for a sufficient duration or was not carried out adequately.

The influence of the compactness, and therefore of the mass of the ballast, is shown later in the graphs of the sections 3.5 and 3.6.

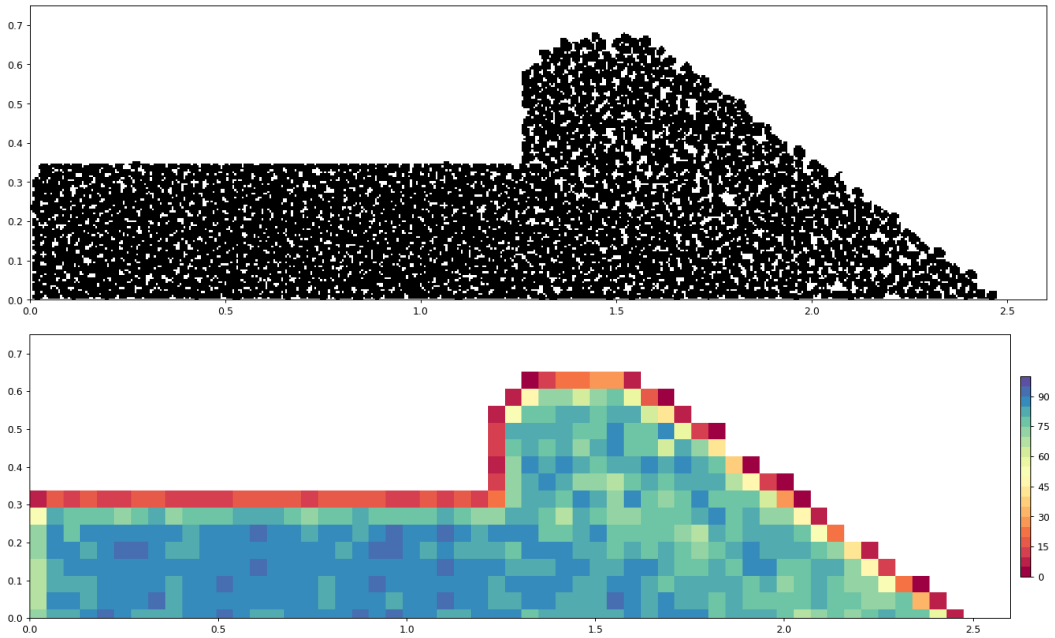

Figure 3.11 – Second model studying the lateral resistance. The unit of measure is the meter

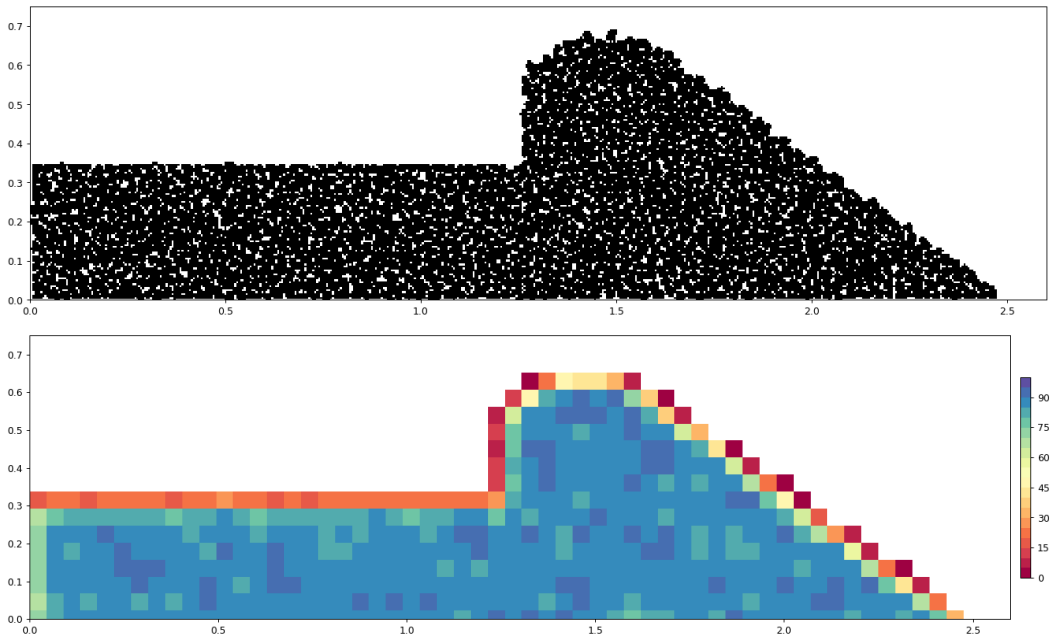

Figure 3.12 – Third model studying the lateral resistance. The unit of measure is the meter

3.5 Comparison of the lateral resistance

In the first model represented in figure 3.14, the studied ballast presents a practically uniform compaction, even on the side of the sleeper. In the graph below, the relation

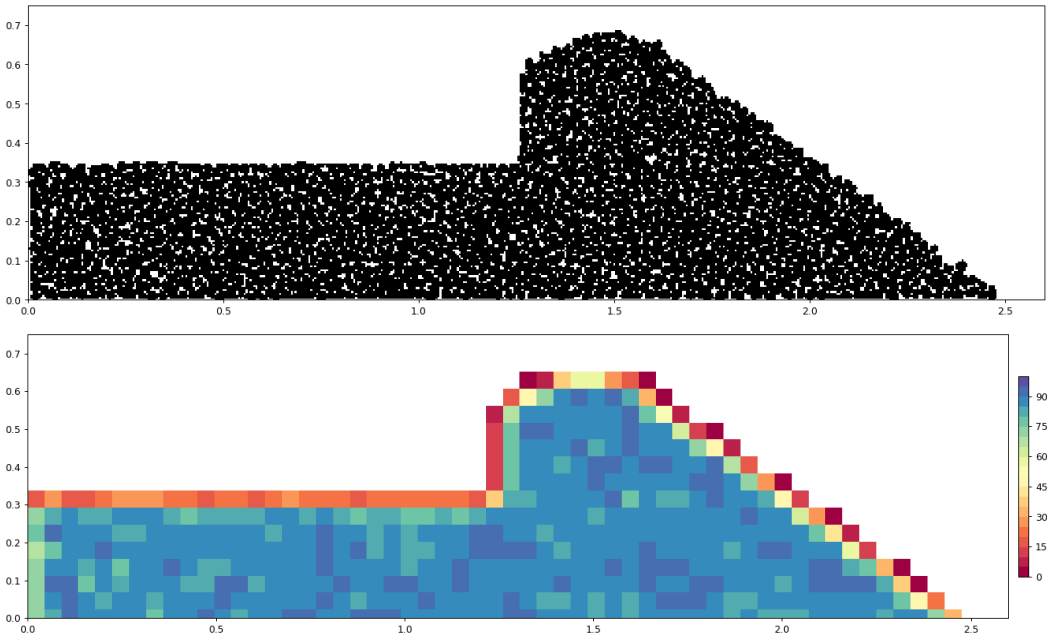

Figure 3.13 – Fourth model studying the lateral resistance. The unit of measure is the meter

Table 3.1 – Summary of the simulations for the lateral resistance

Name	Compaction	Type of imposed displacement	Value	Friction (grains)	Friction (ballast-sleeper)
Fig. 3.14	Below and beside	Velocity (2 mm/s)	10 mm	0.7	0.5
Fig. 3.15	Below	Velocity (2 mm/s)	10 mm	0.7	0.5
Fig. 3.16	Below	Velocity (2 mm/s)	50 mm	0.7	0.5
Fig. 3.17	Below	Incremental force ($\Delta F = 1.5$ N)	10 mm	0.7	0.5
Fig. 3.18	Below	Velocity (2 mm/s)	10 mm	0.8	0.5
Fig. 3.19	Below	Velocity (2 mm/s)	10 mm	0.8	0.7
Fig. 3.20	Below	Incremental force ($\Delta F = 2$ N)	10 mm	0.8	0.7
Fig. 3.21	Below	Incremental force ($\Delta F = 1$ N)	10 mm	0.8	0.7

between the applied force and the movement of the sleeper was represented, that is the force necessary for the sleeper to overcome the resistance of the ballast to its side and be able to move. The lines represent the four different profiles of the ballast and the

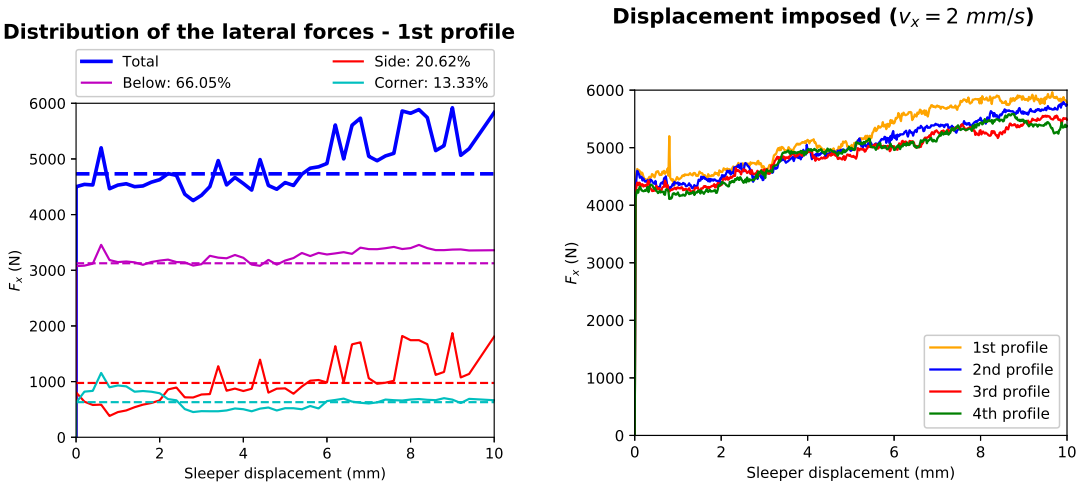

(a) *Influence of the forces in the different zones of the ballast*

(b) *Lateral resistance of the ballast*

Figure 3.14 – Lateral resistance of a ballast compacted below and beside the sleeper, subjected to a constant displacement

differences are not high.

In the second model, the ballast is compact below the sleeper while it has a lot of empty spaces on the side and therefore less resistance of the ballast is expected. As can be seen in figure 3.15, the resistance that this ballast opposes to the movement of the sleeper is much lower than the values of the previous model.

Through a Python script, the forces applied by the sleeper are studied in order to understand which forces act under the sleeper, on the side or in the corner. It has been decided to insert also the force corresponding to the corner because if a stone is present in that position it is not known with certainty if this stone is below the sleeper or beside. In the following graphs, it has been chosen to represent only the first profile.

To calculate the percentage of forces in the different zones, a different procedure is used for longer time intervals, making the calculation of the graph on the left less accurate. In fact, not always the blue line of the graphs on the left coincides perfectly with the yellow line of the first profile of the graph on the right. However, the calculation of the percentages proves to be accurate.

Obviously, since the area of the base of the sleeper is greater, the forces applied under the sleeper have a greater percentage, followed by the forces on the side of the sleeper and those on the corner.

The graph in figure 3.15 analyses the forces applied in another ballast with compaction under the sleeper and not compacted on the side. As might be expected, a ballast of

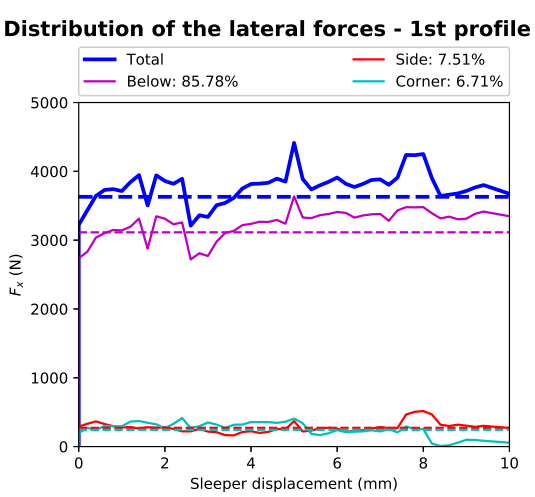

(a) *Influence of the forces in the different zones of the ballast*

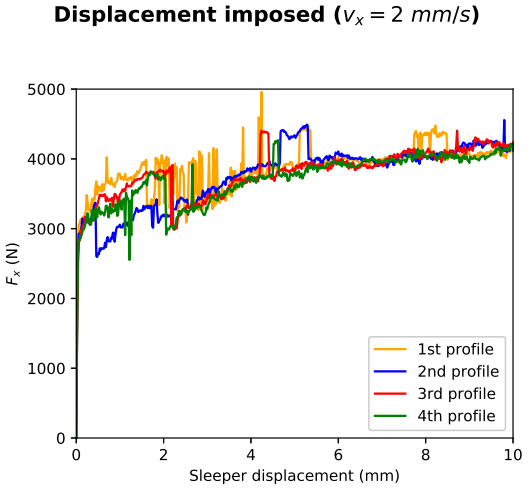

(b) *Lateral resistance of the ballast*

Figure 3.15 – Lateral resistance of a ballast compacted below, subjected to a constant displacement

this kind offers greater resistance to the base of the sleeper, and less to the side. In fact, calculating these forces, the difference is overwhelming: 86% of the forces are below, 8% at the sides and 6% at the corner.

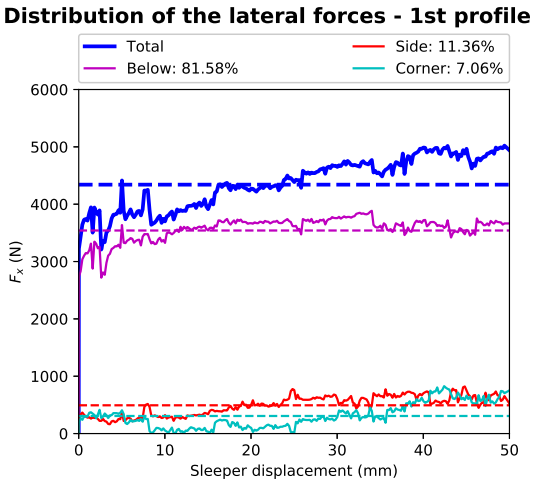

(a) *Influence of the forces in the different zones of the ballast*

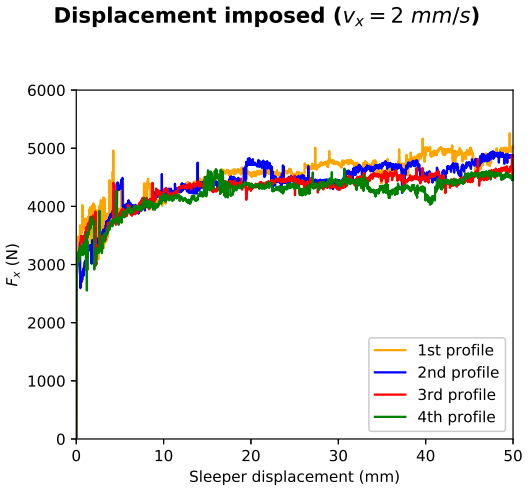

(b) *Internal view of the tamping machine*

Figure 3.16 – Lateral resistance of a ballast compacted below the sleeper, subjected to a constant displacement

The two graphs in figure 3.16 show the movements before up to a maximum of 50 mm.

The ballast is particularly compact and at first sight, it would seem that the side of the sleeper is more compact than the part below. Looking at the graphs it can be noticed a constantly increasing shift at the side of the sleeper for the first 15 mm, after which there is a constant trend of the force. Also, in this case, the difference between the first ballast profile and the last one is clear, while the difference between the first and the second is not particularly evident. Indeed, for short moments the values of the second profile reach those of the first and in some instants are even greater.

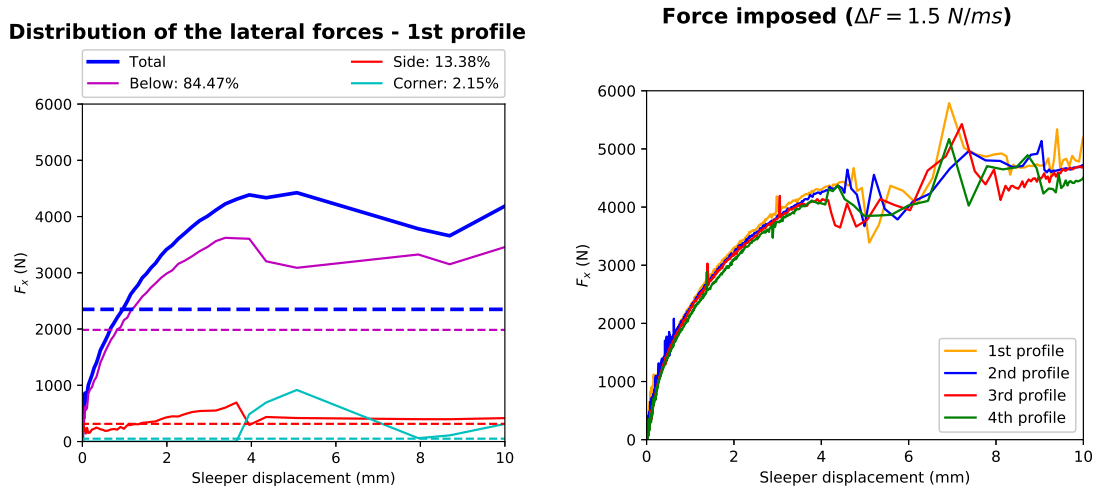

(a) *Influence of the forces in the different zones of the ballast*

(b) *Lateral resistance of the ballast*

Figure 3.17 – Lateral resistance of a ballast not compacted beside the sleeper, subjected to an incremental force

In the simulation showed in the figure 3.17, the sleeper was pushed by an increasing force of 1.5 N/ms, until the reaching of a total displacement of 10 mm. This type of force allow the reader to view a first logarithmic phase, but subsequently it is followed by a phase with many oscillations, most likely due to the fact that the force increase of 1.5 N/ms is too high.

In the simulation showed in the figure 3.18, the sleeper was pushed by a constant velocity of 2 mm/s, until the reaching of a total displacement of 10 mm. The friction between the grains is increased, from 0.7 to 0.8. The only difference between this simulation and that one showed in the figure 3.15 is that the friction between the grains changed. As in the reality, the resistance is bigger but not in an important way.

In the simulation showed in the figure 3.19, the sleeper was pushed by a constant velocity of 2 mm/s, until the reaching of a total displacement of 10mm. The friction between the grains is 0.8 and the friction between the ballast and the sleeper is increased, from 0.5 to 0.7. Here the difference between the graph in figure 3.15 is more evident, because the increasing of the friction increase the stability of the track.

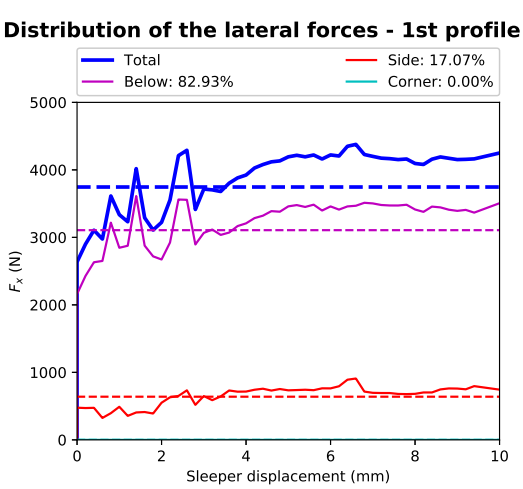

(a) *Influence of the forces in the different zones of the ballast*

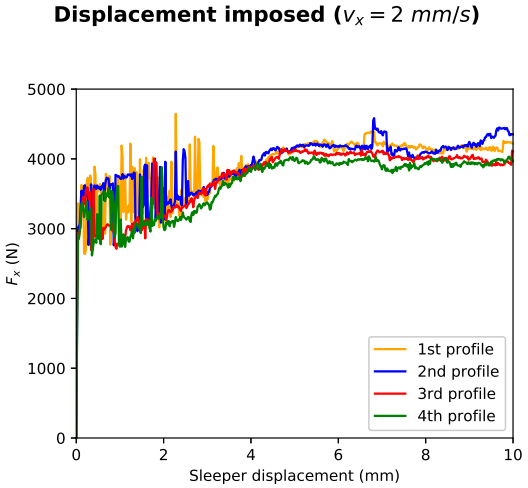

(b) *Lateral resistance of the ballast*

Figure 3.18 – Lateral resistance of a ballast not compacted beside the sleeper, subjected to a constant displacement

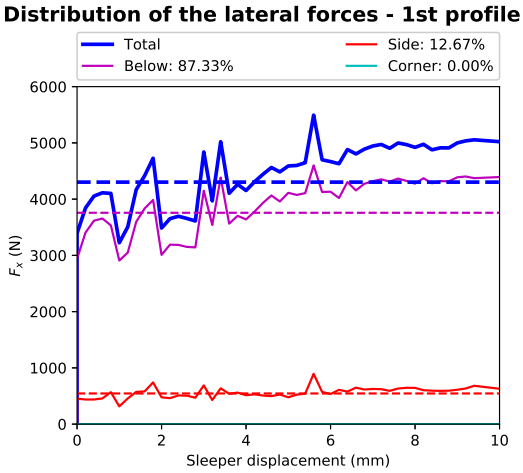

(a) *Influence of the forces in the different zones of the ballast*

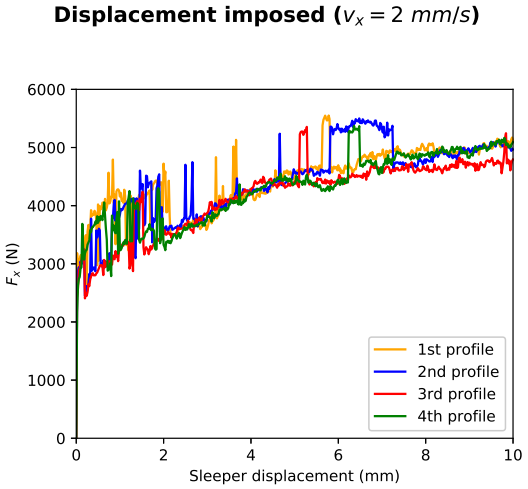

(b) *Lateral resistance of the ballast*

Figure 3.19 – Lateral resistance of a ballast not compacted beside the sleeper, subjected to a constant displacement

In the simulation showed in the figure 3.20, the sleeper was pushed by a constant force of 2 N/ms, until the reaching of a total displacement of 10 mm. The friction between the grains is 0.8 and the friction between the ballast and the sleeper is 0.7. As in the figure 3.17, there is a main phase with a logarithmic behaviour, followed by some oscillations. The step of the incremental force is even bigger and should be rejected, but it is possible

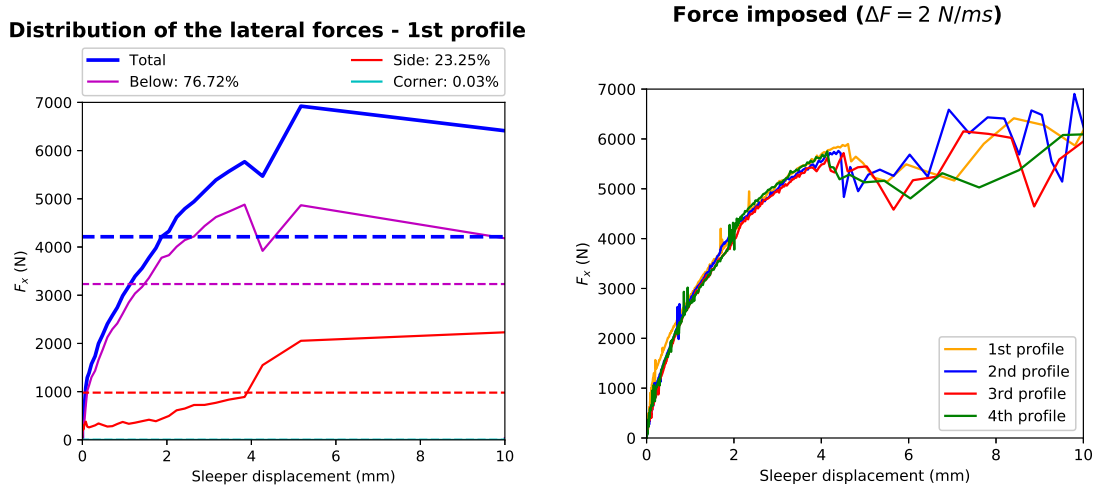

(a) *Influence of the forces in the different zones of the ballast*

(b) *Lateral resistance of the ballast*

Figure 3.20 – Lateral resistance of a ballast not compacted beside the sleeper, subjected to an incremental force

to observe that the resistance reach bigger values.

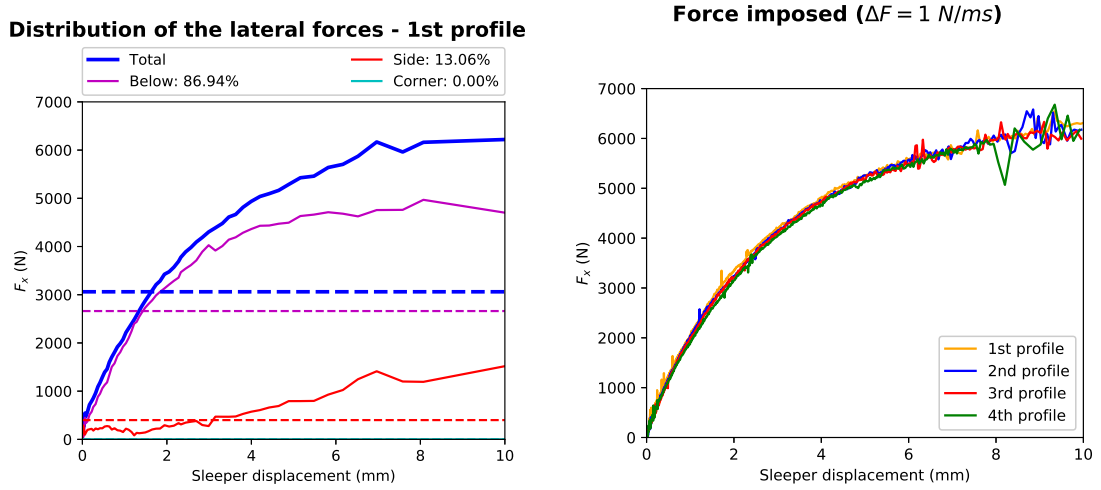

(a) *Influence of the forces in the different zones of the ballast*

(b) *Lateral resistance of the ballast*

Figure 3.21 – Lateral resistance of a ballast not compacted beside the sleeper, subjected to an incremental force

In the simulation showed in the figure 3.21, the sleeper was pushed by a constant force of 1 N/ms, until the reaching of a total displacement of 10 mm. The friction between the grains is 0.8 and the friction between the ballast and the sleeper is 0.7. In this graphs

there are no oscillations and also in this case there is a logarithmic phase followed by a linear one.

A summary that helps to understand the simulations performed is included in the table 3.1.

3.6 Influence of the mass

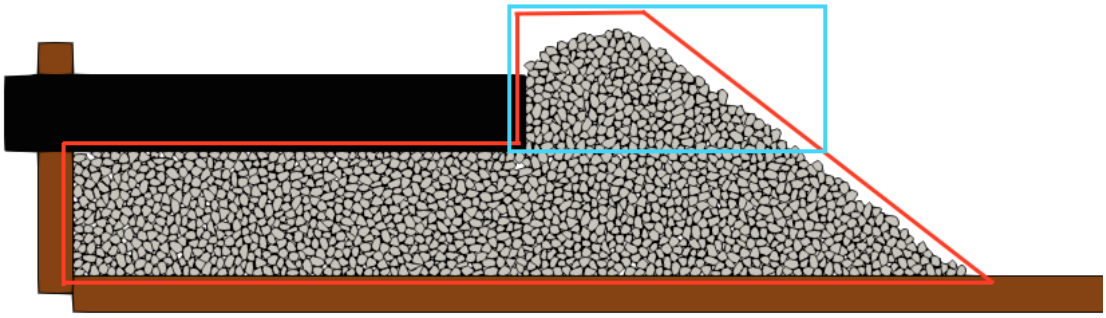

Figure 3.22 – Scheme of the mass beside and below the sleeper (red) and beside the sleeper (cyan)

The profiles of the ballast are important because the lateral resistance of the ballast depends on them. But in this simulation, how much do they affect? Is it normal that there is not a big difference between the profiles?

The problem is that there is a visible difference in some graphs, for example in the figure 3.16, but it is not so evident. In this phase of the work the linear mass of the total ballast (beside and below the sleeper) was computed and it was compared with the mass next to the sleeper of the four profiles.

The stones located in the red area are the stones belonging to the mass of the total ballast, while the stones in the cyan area belongs to the stones analysed for the four different profiles beside the sleeper. As an example, the first profile is shown in figure 3.22.

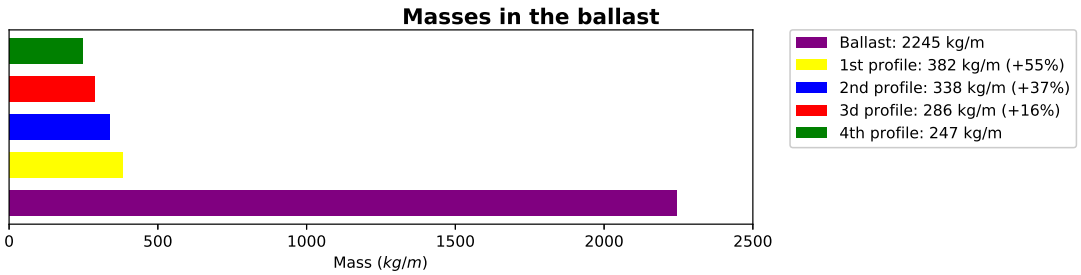

Figure 3.23 – Comparison of the masses of each profile with the total mass of the ballast with the not compacted zone

In the case of a ballast compacted below the sleeper and not compacted beside the sleeper, the difference of the linear mass between the first and the fourth profile is about a +55%, but it is not so big compared to the mass of the total ballast with the first profile.

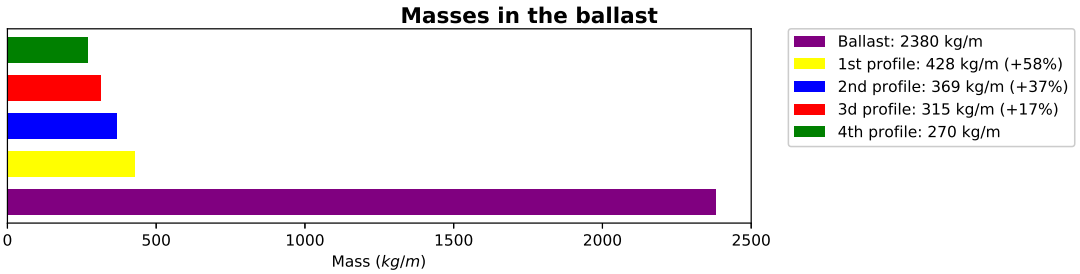

Figure 3.24 – Comparison of the masses of each profile with the total mass of the ballast where everything is compact.

In the case of a ballast compacted below and beside the sleeper, the difference of the linear mass between the first and the fourth profile is about a +58%, and in general, the masses are higher, so the ballast has a better stability, but also in this case the influence of the mass is not important.

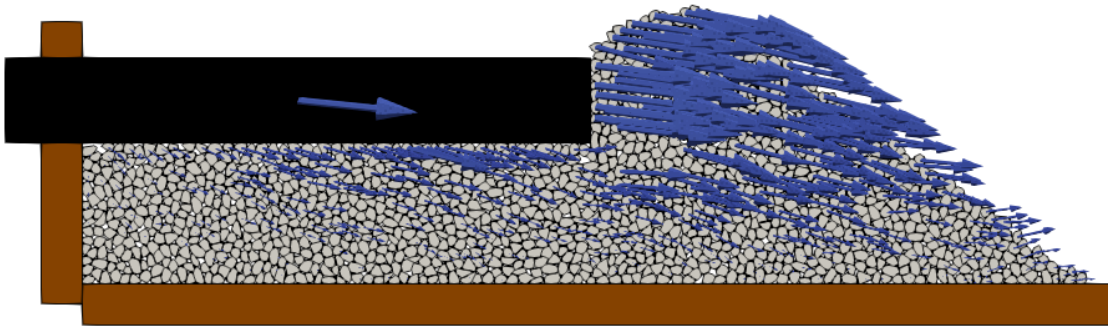

Figure 3.25 – Velocities of the different bodies in a ballast compacted everywhere

When the sleeper moves the grains, the ballast is divided into two parts: a part that remains stationary and a part that is displaced. It is difficult to say precisely which stones are displaced and which are not because this can vary in the various moments of the simulation. Looking at the figure 3.25, the arrows that indicate the speed of all the bodies in the simulation. From this point of view, it would seem that the subdivision used to calculate the various masses is suitable, but to obtain with extreme precision the amount of mass displaced is very difficult.

The difference in mass between the first and the fourth profile for the case in which every zone is compacted is 158 kg. The frictional force that opposes the movement of a mass is:

$$T = \mu \cdot \Delta m \cdot g = 0.7 \cdot 158\ kg/m \cdot 9.81\ m/s^2 = 1\ kN/m \tag{3.3}$$

The coefficient of friction, for this short calculation, is set equal to 0.7, but this is a great approximation.

As shown in figure 3.14, the difference between the resistance of the first and fourth profiles is around 1 kN, so the model seems valid.

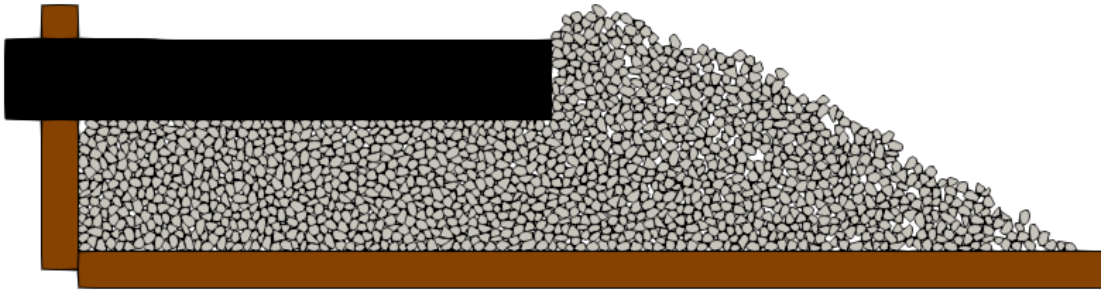

Figure 3.26 – A ballast compacted only below the sleeper after the 10 mm displacement

Regarding the other case, the lack of difference between the various profiles is not very accentuated because when the sleeper moves the stones to its side they are not compacted, so they tend to fall to the sides more easily (fig. 3.26), reducing the mass of each profile and the lateral resistance is therefore less.

3.7 Comparison with experimental results

Section 3.1 discussed the test carried out by TU Delft's Roads and Railways. The differences at the base between the simulations and this test are that it presents much higher resistance values and the lateral displacement is imposed up to 200 mm. In addition, the speed set by the sleeper is 10 mm/min, much lower than the speed set in the simulation, equal to 2 mm/s.

Obviously, obtaining the conditions of compactness identical to the test carried out in the laboratory is very difficult, it should also be remembered that the coefficients of friction and the 2D representation of the stones greatly influence the numerical values of the simulations.

From a general point of view, however, it is possible to notice a transitory trend in the first part of the simulation and finally an asymptotic pattern (figure 3.2).

In conclusion, the discrete element method and the LMGC90 software allow performing simulations that show a difference when there is a difference in compaction and a different friction between the bodies. As would be expected, in the simulation where the ballast is compact, the values of the forces calculated below the sleeper influence with a lower percentage compared to the same type of forces obtained in the model in which there is a non-compact area. In the second type of simulation, in fact, the area below the

sleeper, being more compact, opposes a greater resistance to the sliding of the sleeper and therefore influences with percentages around 80-90%.

4 Vertical settlement

4.1 Experimental models

In this second part of the thesis, the behaviour of the ballast and the elastic layers placed below the sleeper and above the platform are studied under vertical loads with the discrete element method. The results of a real model are compared to the results obtained from the software.

The model is that one realised by the *Centre d'Essais et d'Expertises* of the SNCF, the France's national state-owned railway company, linked to the Juan Carlos Quezada's thesis. [17, 16] There is a vertical load over a track placed between two monoblock concrete sleepers, with an elastic layer placed under the ballast. The loads applied go from a minimum of 48.5 kN to a maximum of 68.1 kN, with an average value of 59.7 kN, trying to simulate the forces behaviour during a train transition. Juan Carlos Quezada used two values of stiffness for the elastic layer: 12 and 500 MPa. In regards to the frequencies of the charge, he used 3.3 , 4.5 , 5.4 and 6.0 Hz, that are the equivalent of the speeds 220 , 300 , 360 and 400 km/h. [17, 16]

4.2 Implementation of the model in the software

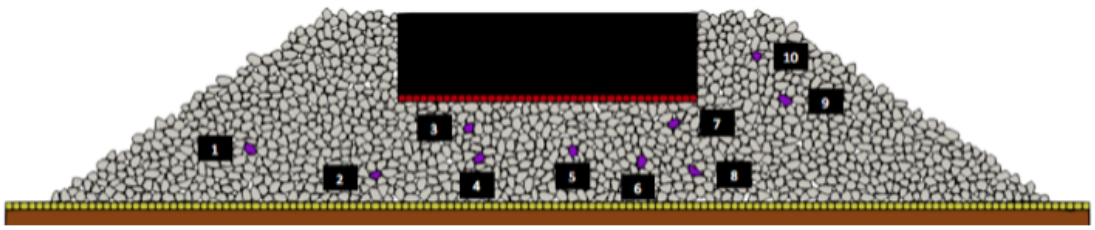

Figure 4.1 – Numerical model to simulate the settlement of the sleeper

The second simulation model analyses the vertical settlement of the sleeper. This is a

much longer simulation because it lasts 320 seconds. In addition, the entire ballast is studied and therefore no longer its half. On average, the time to perform a simulation of this type is one and a half days but it varies depending on the number of stone to be saved. For this simulation, it was decided to model three different tracks:

- A track with an elastic layer in the bottom of the ballast;
- A track with an elastic layer in the bottom of the ballast and below the sleeper;
- A track without elastic layers.

Two values of stiffness were then added to the simulation, each for each layer above and below the ballast. From the technical documents of Infrabel the following values have been used: [4, 5]

- $k_1 = 0.035\ N/mm^3$ for the elastic layer positioned above the platform;
- $k_2 = 0.300\ N/mm^3$ for the elastic layer positioned under the sleeper.

In the model, being a discrete element simulation, each elastic layer is modelled with small squares of 20 mm on each side, and being in the two-dimensional model, the depth is equal to one meter. So the values entered in the simulation are the following:

- $k_1 = 0.035\ N/mm^3 \cdot 20\ mm \cdot 1000 = 7 \cdot 10^5\ N/m$
- $k_2 = 0.300\ N/mm^3 \cdot 20\ mm \cdot 1000 = 6 \cdot 10^6\ N/m$

These samples representing the various types of track were created by first placing all the stones in a large container (fig. 4.2) where this time the whole track is represented and not just half the portion. The upper artificial walls and the stones are allowed to fall by gravity, while all the other bodies remain fixed (fig. 4.3). The upper walls, therefore, apply a constant force equal to its weight, or 2575 N.

The second profile (fig. 1.8) of the Infrabel ballast is assigned to each track, i.e. the one for high-speed trains. The upper and lateral artificial walls and the stones outside this profile are therefore rendered invisible (fig. 4.4). The last step is the application of the vertical load (fig. 4.5) on the concrete sleeper: it is the passage that undergoes more variations between one simulation and the other because it can be chosen to study only the settlement, that is the vertical displacement of the sleeper, or even the horizontal displacement and its rotation.

The force applied to the sleeper is applied for a duration of 200 seconds, which identifies this step as the longest one. The force is sinusoidal and has two different equations. The first oscillates between 3 and 32 kN, with a frequency of 10 Hz. It is obviously applied downwards and starts at a value of 3 kN to not immediately have a situation too loaded, which could damage the model. [17] The equation of force introduced in the simulation

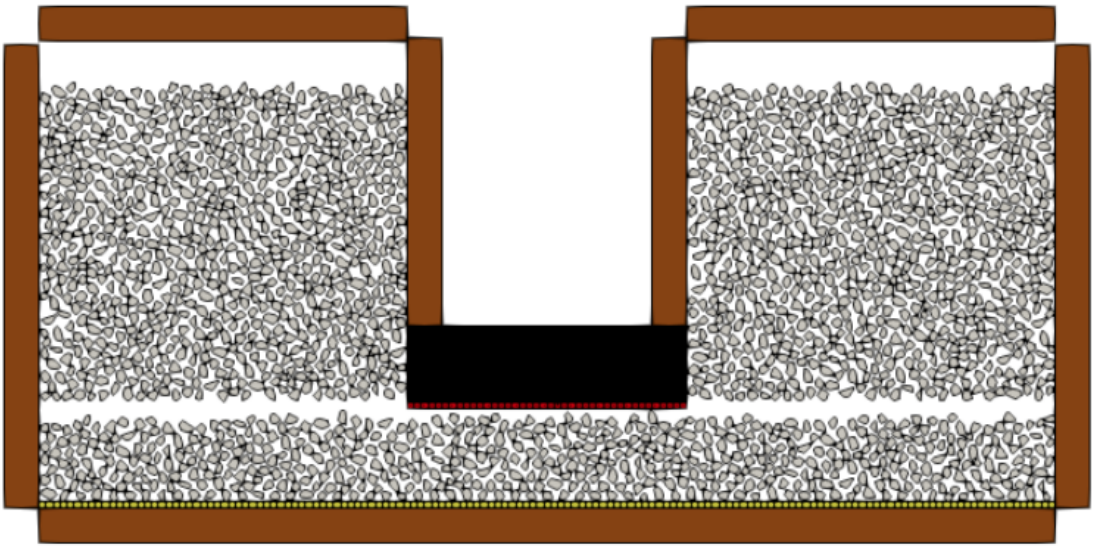

Figure 4.2 – First phase: placement of the stones in the box

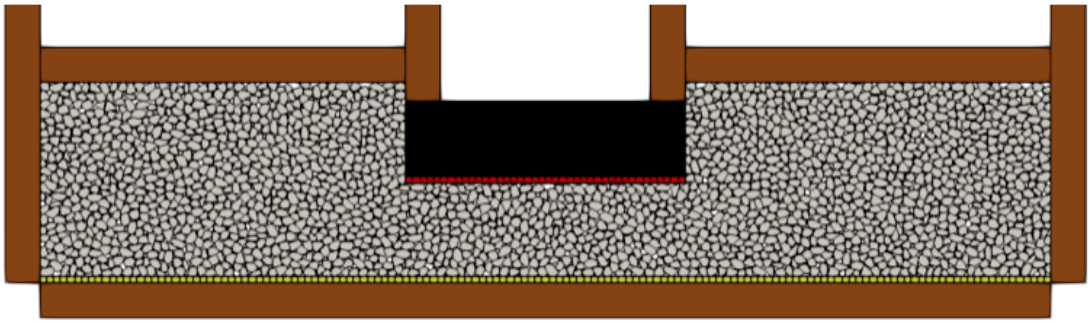

Figure 4.3 – Second phase: compaction of the stones in the box

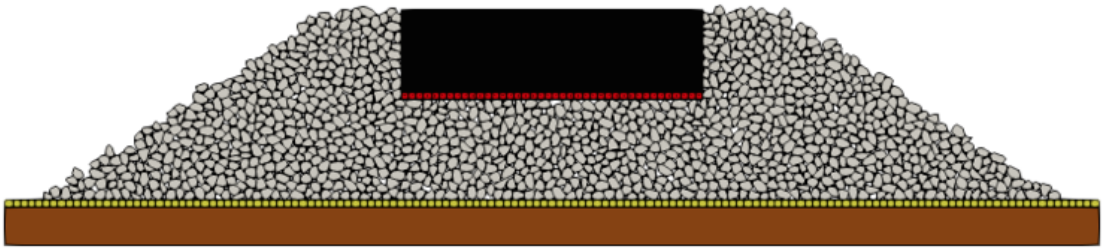

Figure 4.4 – Third phase: hiding of the stones to create the ballast profile

and its graphical representation are the following:

$$F(t) = A \cdot [1 - \cos(2\pi f t)] + F_{min} \tag{4.1}$$

Where:

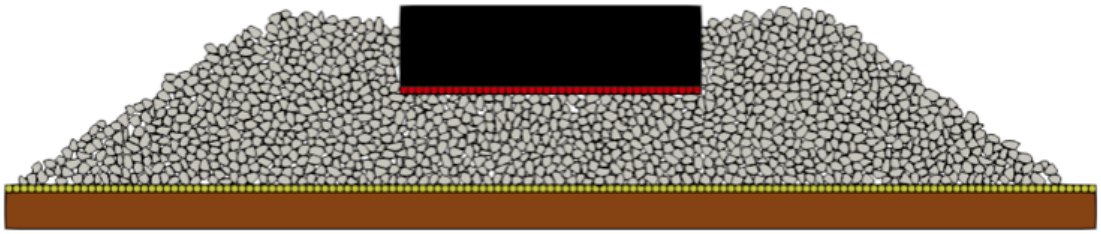

Figure 4.5 – Fourth phase: a vertical force is imposed to the sleeper

- A is the amplitude: $(F_{max} - F_{min})/2$
- F_{max} is the maximum force: 32 kN;
- F_{min} is the minimum force: 3 kN;
- f is the frequency: 10 Hz;
- t is the time, in seconds.

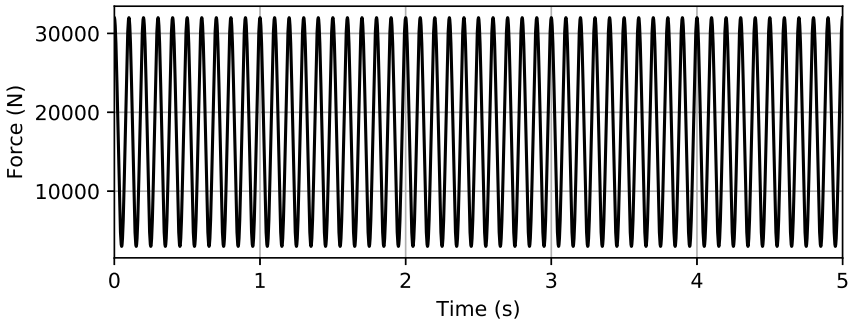

Figure 4.6 – Numerical model to simulate the settlement of the sleeper

The second force used for the application of the load has the following equation:

$$F(t) = \frac{F_{max}}{2} \cdot \left[1 + \left(2\pi \cdot \left(f_0 + \frac{f_1 - f_0}{t_1 - t_0} \cdot \frac{t}{2}\right) \cdot t\right)\right] \tag{4.2}$$

This is the frequency sweep equation, and unlike the previous one, it was used to study the behaviour at various frequencies.

Where:

- F_{max} is the maximum force: 32 000 N;
- f_0 is the initial frequency: 20 Hz;
- f_1 is the final frequency: 50 Hz;
- t_0 is the initial time: 0 s;
- t_1 is the final time: 200 s.

The graph in figure 4.7 shows the force graph for the first 20 seconds.

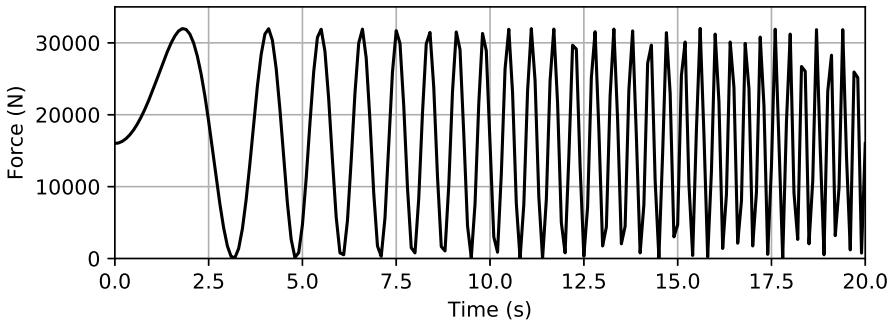

Figure 4.7 – Force graph with a frequency sweep

4.3 Acceleration analysis

Through the LMGC90 software, it is possible to choose which elements to study in greater detail. In particular, by indicating the number that identifies the body, it is possible to visualise the time step, the x, y and z positions of the body and the velocities along the three axes.

It has been chosen to derive the accelerations of some stones at specific points, to analyse how the acceleration varies in the different areas of the ballast and subsequently to compare them with a theoretical model, using only the equations of mechanical physics.

The software does not directly store accelerations, so central-difference formulas need to be used. [8] In particular, it is possible to obtain the value of the acceleration in a specific point, knowing that acceleration is the first derivative of velocities, and using the value in that given time step as a step h.

$$u'(0) = \frac{-U_{2h} + 8U_h - 8U_{-h} + U_{-2h}}{12h} \tag{4.3}$$

With these equations, accelerations of the stones in the different zones of the ballast can be plotted (figure 4.8). In this example the ten stones' accelerations were studied and for each studied stone a number was assigned (figure 4.1). It can be immediately seen that the stones with the greatest accelerations are under the sleeper, and for the stones away from it, the accelerations decrease. The stones placed above platform do not have a high acceleration, probably due to the fact that most of the force applied to the sleeper does not contribute to the profile of the ballast at the sides of it. Also in the graph showing the speed distribution (figure 4.9), there is a tendency similar to that of accelerations: the stones near the sleeper have a greater velocity than those placed far from it. In addition, the six stones placed under the sleeper have an average value almost equal.

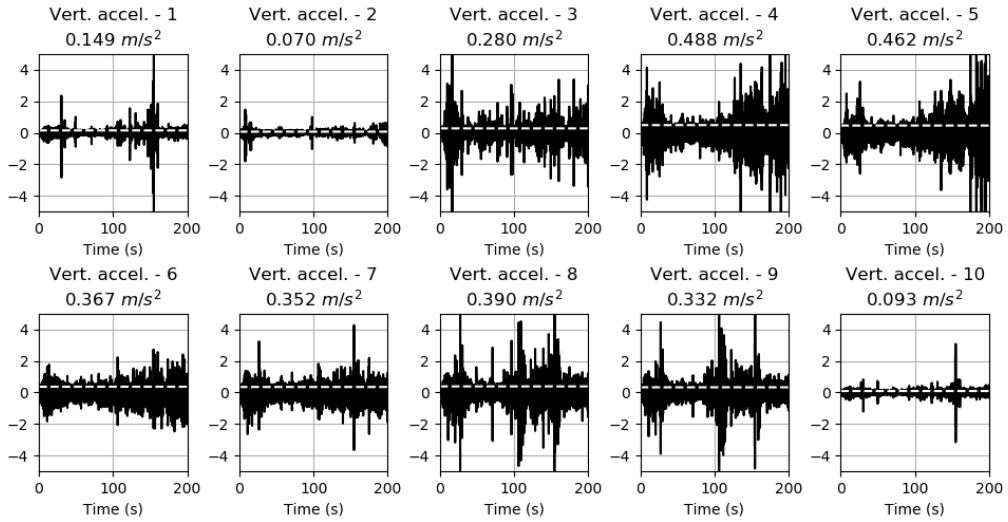

Figure 4.8 – Accelerations of the stones in the ballast

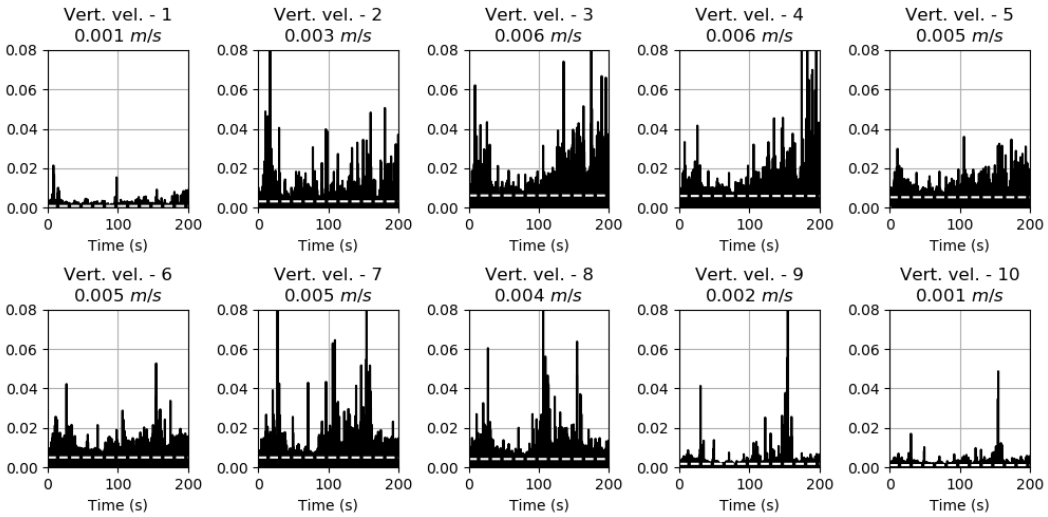

Figure 4.9 – Velocities of the stones in the ballast

In the previous graphs the root mean square (RMS) was calculated:

$$x_{RMS} = \sqrt{\frac{1}{n} \cdot \left(x_1^2 + x_2^2 + \cdots + x_n^2\right)} = \sqrt{\frac{1}{n} \cdot \sum_{n=1} x_n^2} \tag{4.4}$$

The value is positioned above each graph and is represented with a dashed white line. It has been chosen to use this type of mean because both accelerations and velocities have a waveform, and therefore the only arithmetic mean would not have been suitable.

Through Paraview, a software to visualise the data obtained from the simulations with LMGC90, it is possible to obtain a scale representation of the speeds of the stones

placed in the ballast. There are three different moments shown in the appendix C: at the beginning of the simulation, at half simulation and at the end of the simulation.

In general, it is possible to see that the sleeper and its stones positioned below have a higher speed than the others. On the sides of these stones, there is an area where the stones tend to converge towards the centre of the platform, pushing, in turn, the remaining stones, which move towards the external part of the ballast with very reduced speed.

In the immediate start of the simulation, the speeds are higher, probably due to the brusqueness of the forces applied to the sleeper. Then the accelerations approached the average value with peaks, represented by arrows of greater size.

In this model, it was chosen to represent also the accelerations of the sleeper, together with its speed and settlement (figure 4.10). As would be expected, the sleeper has the root square values of acceleration and higher velocity, respectively equal to $0.367\,\mathrm{m/s^2}$ and $0.005\,\mathrm{m/s}$.

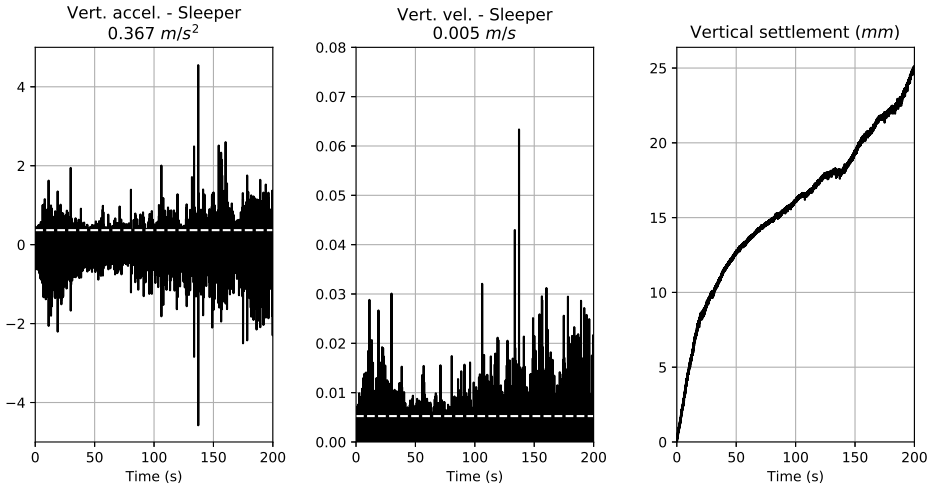

Figure 4.10 – Acceleration, velocity and settlement of the sleeper pushed by a constant frequency force

The total settlement is 25 mm for a simulation lasting 200 seconds. It can be observed that also the graph of the settlement of the sleeper has oscillating values (figure 4.11).

4.4 Settlement of the sleeper

In the figure 4.12, the settlement of the sleeper of four simulations was represented.

- The blue line represents the model in which no elastic layers are placed;
- The orange line represents the model in which an elastic layer is placed only above

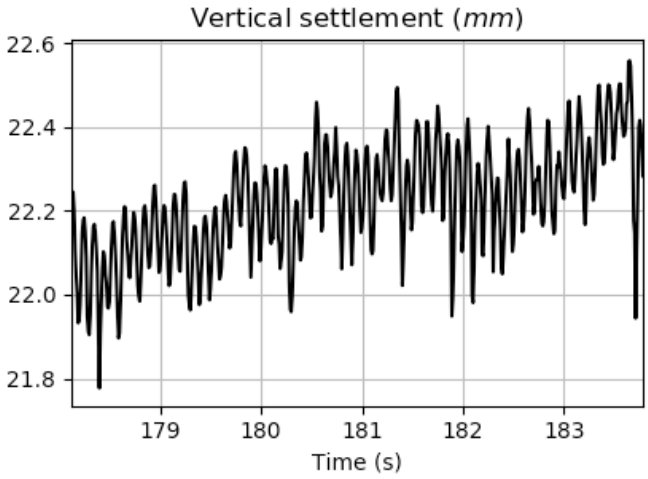

Figure 4.11 – Zoom of the vertical settlement of the sleeper pushed by a constant frequency force

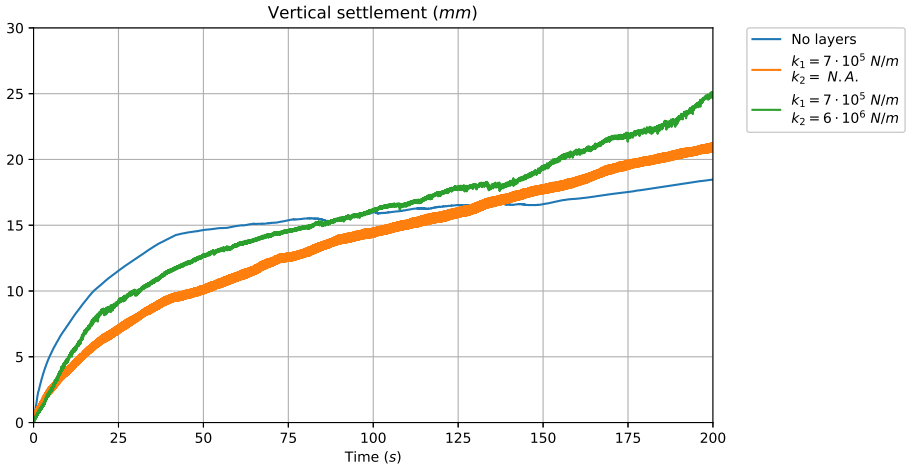

Figure 4.12 – Settlements of the sleepers pushed by a constant frequency force, for the cases with no elastic layers, one elastic layer, two elastic layers

the platform;

- The green line represents the model in which there are two elastic layers: the first above the platform and the second below the sleeper;

First of all it is necessary to specify that the different thickness of the lines is due to the fact that one or more elastic layers is placed. In these cases, with a one-millisecond step, it can be seen that the sleeper has a high oscillatory behaviour, unlike the first model in which it seems that it always has a settlement downward. The model with the greatest settlement is the last one, i.e. the one in which the sleeper suffers a vertical force downwards by frequency sweep. This, in all probability, is due to the fact that the frequency sweep equation goes from a frequency of 20 Hz to 50 Hz, and then in the final

part receives a greater boost. It can be also noticed, as it could be expected in reality, that increasing the frequency also increases the slope of the graph of the settlement.

The difference with the graph of the settlement of the third model is not so high, only 2 mm. This model has a frequency of 10 Hz and probably the frequency of loading does not have a great influence on the settlement of the sleeper.

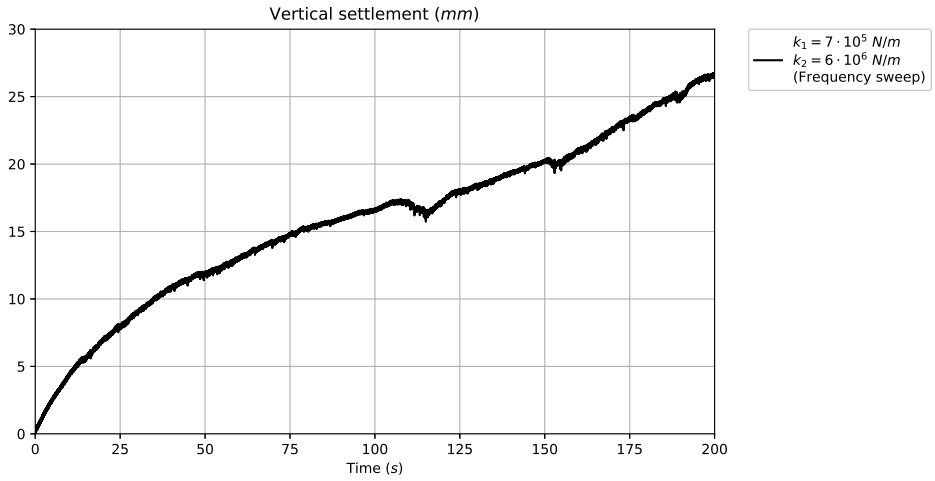

Figure 4.13 – Settlements of the sleepers pushed by a frequency sweep force

The line in figure 4.13 represents the model in which, unlike the others, the frequency sweep equation is used. Like the previous model, it has two elastic layers.

4.5 Comparison of the compactness

Also for this second model, the compactness of the ballast on the sides and below the sleeper has been studied with the aim of analysing the variation of the compaction during this process of creating the model. The images below are the graphic result of the same script used above for the lateral resistance model. Also in this case, there is not a big difference with the image provided by the LMGC90 software.

Figure 4.14 shows the level of compaction preceding the beginning of the application of the vertical force on the sleeper.

Then a force is applied and it is possible to notice that the height of the layer of stones below the sleeper is smaller. The greater compaction occurs at one side of the sleeper (the right side) and below (figure 4.15). This is probably due to the fact that the ballast is not perfectly symmetric, so there is a tendency for stones to move more to one side.

Figure 4.16 shows the movements of the stones before the application of the force and after its application. The green value, with its maximum at 100 %, means that in that

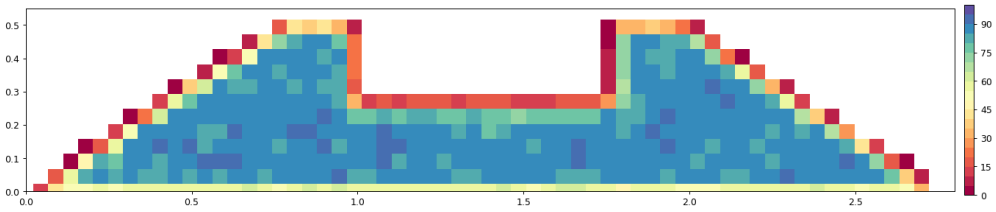

Figure 4.14 – Compactness of the ballast before applying the force to the sleeper. The unit of measure is the meter

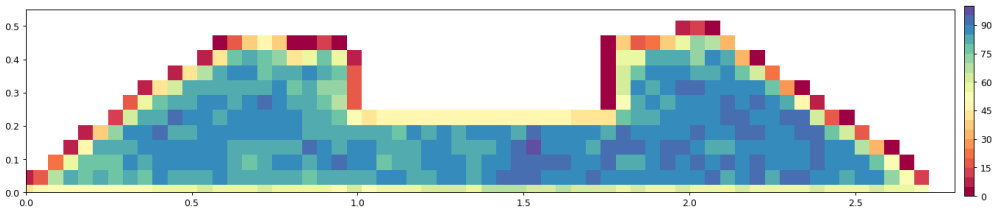

Figure 4.15 – Compactness of the ballast after applying the force to the sleeper. The unit of measure is the meter

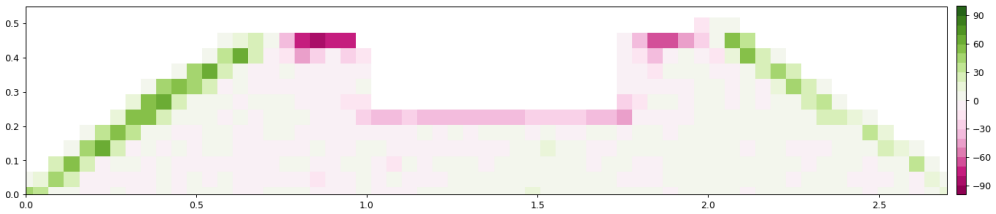

Figure 4.16 – Movement of the stones in the ballast after applying the force to the sleeper. The unit of measure is the meter

area the stone was not there before the application of the force and it is in that position after the compaction. The red values, with its minimum at $-100\,\%$, means that the stone was there only before the application of the force.

As it can seen, the differences are not too high because in the graph there are almost only light colours. Generally, at first glance, the green colour is the most present, therefore with a greater compaction, especially on the sides of the ballast. In fact, after the application of a load on the sleeper, it should be expected a compaction below the sleeper and the movement of the grains to the sides of the ballast. The dark green colour present diagonally on the sides of the ballast represents just this. This concept is also confirmed by the files displayed in Paraview (see appendix C), where it is clearly seen that the vectors of the velocities of the external stones tend to always move outwards, while those near the sleeper tend to fall down. These images also show the oscillations that the bodies have: in a first moment the speeds are directed downwards, then upwards and then immediately downwards again.

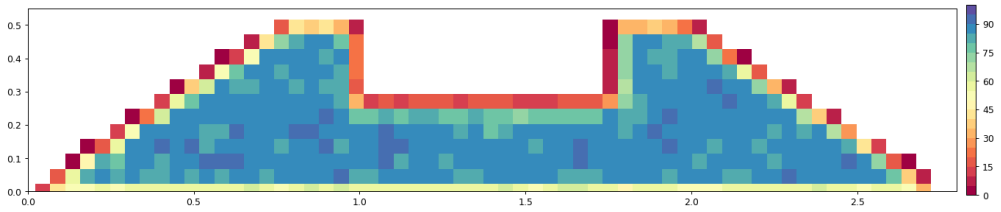

Figure 4.17 – Compactness of the ballast before applying the force to the sleeper. The unit of measure is the meter

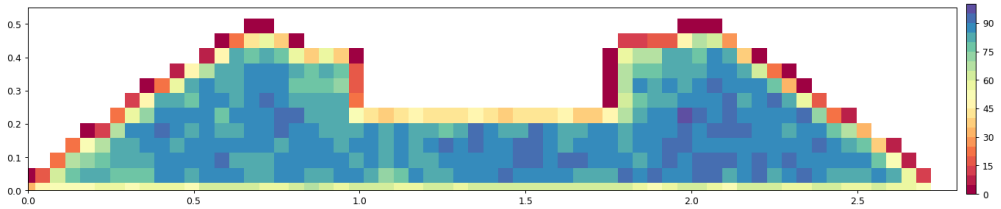

Figure 4.18 – Compactness of the ballast after applying the force to the sleeper. The unit of measure is the meter

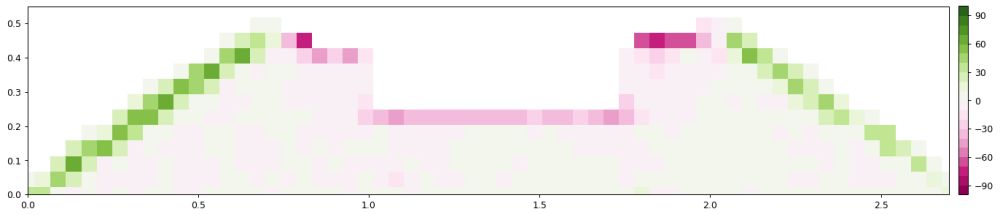

Figure 4.19 – Movement of the stones in the ballast after applying the force to the sleeper. The unit of measure is the meter

4.6 Comparison with a theoretical model

Another aim of this thesis is to find a relationship between a theoretical model, calculable with simple dynamics equations, and a model that can be calculated using the LMGC90 software. For this reason, it is necessary to consider the model consisting of two masses: m_2, i.e. the mass of the sleeper, and m_1, the mass of the ballast. Two elastic components have been added to this model: k_1 or the equivalent elastic component of the elastic layer placed just above the platform, and k_2, the equivalent elastic component of the elastic layer placed just below the sleeper (fig. 4.20).

It is, therefore, a 2D model with only one degree of freedom and through which the vertical displacements were studied, from which the accelerations were subsequently obtained. The latter were compared with the accelerations obtained with the models applied on LMGC90. The demonstration of the calculation of the eigenmodes has been included in the appendix B.

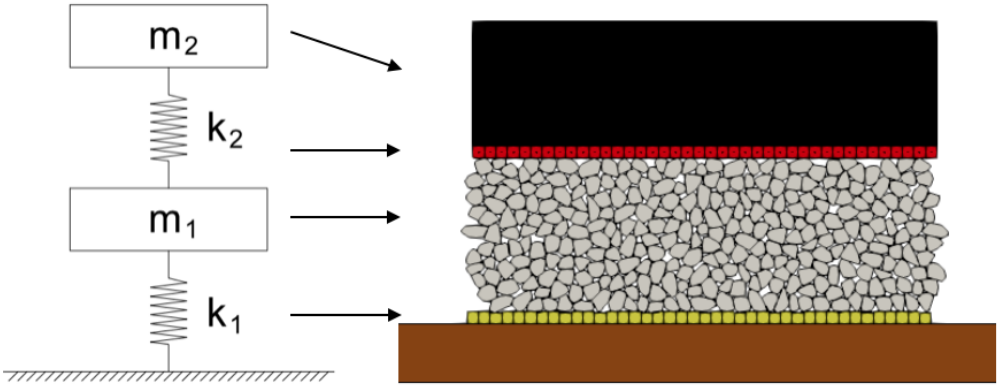

Figure 4.20 – Scheme of a two mass spring system

The sleeper undergoes an oscillating movement, so it is possible to calculate its eigenvectors and eigenvalues. Through the calculation of the eigenvalues, frequency response peaks were obtained at 27 Hz and 164 Hz. Figure 4.21 shows the two graphs of the frequency responses function of the ballast and the sleeper as a function of the frequency.

The model with the sleeper that undergoes a force with a frequency sweep has a range of frequencies ranging from 20 Hz to 50 Hz and therefore it should be expected a greater acceleration of the stones in the ballast and of the sleeper to just half simulation. Looking at the figure 4.22, it can be seen a high acceleration peak. It would seem that the model is valid, but it would be appropriate to carry out a simulation with a constant frequency force applied to the sleeper at 27 Hz and evaluate how the accelerations in the model vary, where presumably will be greater.

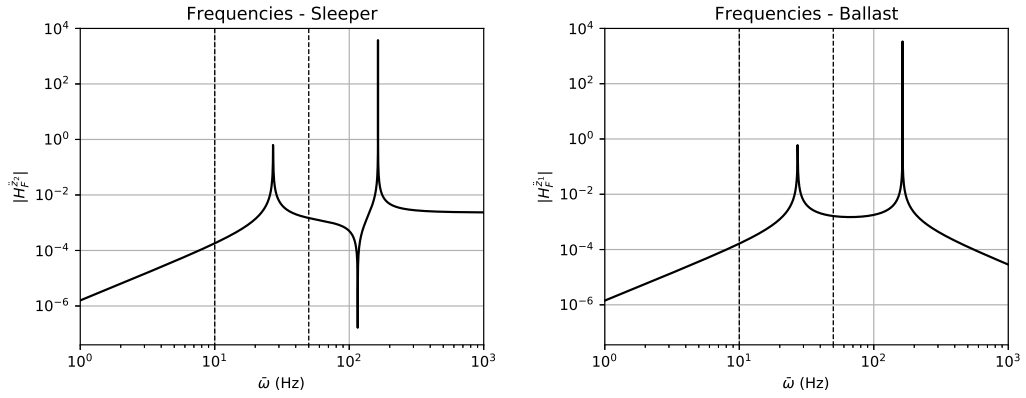

Figure 4.21 – Frequency response functions

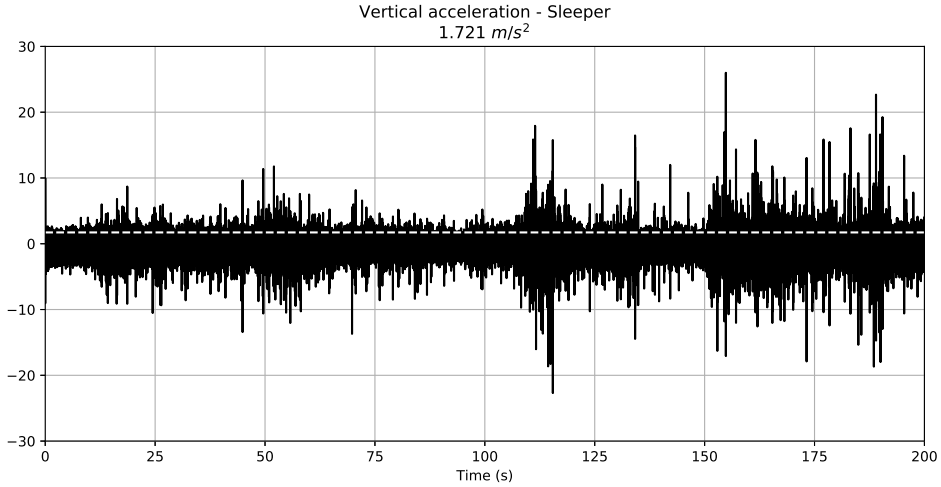

Figure 4.22 – Acceleration of the sleeper loaded by a frequency sweep

4.7 Results for the ballast in the box

In Raül Acosta Suñé's thesis, [17] the settlement of the ballast was simulated in a box with vertical walls, for a duration of 360 seconds, with and without the addition of an elastic layer above the platform. Figure 4.23 shows the vertical displacements as a function of time for situations with and without the elastic layer. Also in this case the settlements are considered positive.

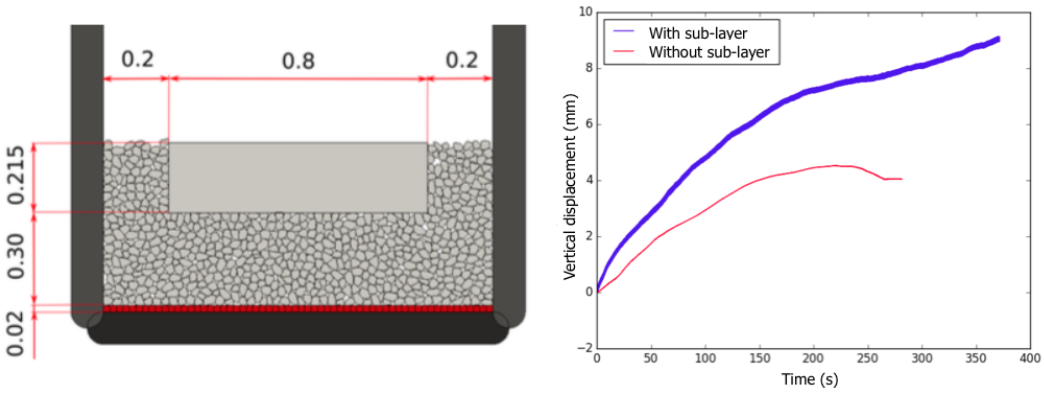

Figure 4.23 – Settlement of a sleeper placed in a box (translated [17])

It can be observed a more oscillatory behaviour for the situation with the layer placed above the platform because that has an elastic behaviour. This is the reason why the stones undergo a more oscillating movement contrary to the situation without the elastic layer. At the end of the simulation, the blue curve without continuing to increase, while, for the red curve, the displacement seems to have stopped. [17] It is possible to notice that the settlements obtained are lower than the settlements shown in figure 4.12. This is due to the fact that the stones are placed in a large box and therefore the wall-stone

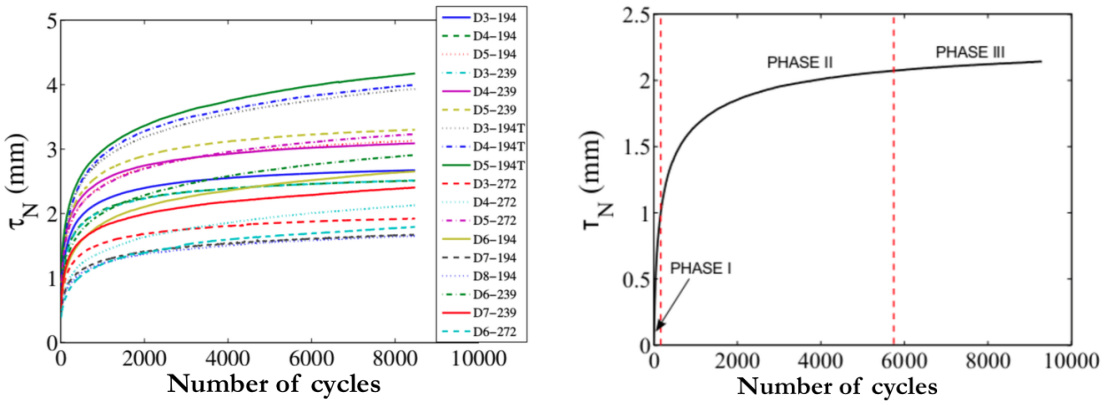

(a) *Settlement curves for each test* (b) *Three phases of settlement in the curve*

Figure 4.24 – Vertical settlement of the sleeper as a function of the number of cycles in the experimental model (translated [16])

friction plays a fundamental role.

4.8 Comparison with the experiences

As it can be seen in the figure 4.24, the shape of the curve obtained from the Juan Carlos Quezada's thesis [16] is very similar to the curve obtained from the software LMGC90 (fig. 4.12). It could be seen that there are three main phases in a settlement curve, as explained before: a first linear phase, the logarithmic phase with a point of inflexion and the linear phase. All these phases can be found in the simulations carried out and shown previously.

Obviously the numerical results are not the same. This is due to the friction coefficients, the type of compaction, the type of force applied to the sleeper and also due to the fact that the model is 2D.

Conclusions and perspective

General conclusions

A plenty of simulations were carried out during these months through the software LMGC90, with a high number of data as results. The simulations focused on the importance of the ballast layer of the track and, as explained in the previous chapters, some parameters can totally change the results.

In the first part, the simulations studied the lateral resistance of the ballast that in general is caused by the buckling effects of the welded rails subjected to a prevented dilatation. Afterward, the settlement of the sleeper is studied because it is caused by the train traffic.

For what concerns the first analysis, the software has shown that there is a difference between the four profiles of studied ballast and the effect of compaction. When there is a ballast reinforced with a protuberance, a graph has been obtained and it showed a greater resistance. Moreover, it has been shown that a compact ballast has a greater resistance than a not-compacted ballast and that increasing the compactness decreases the influence of forces below the sleeper.

The software also showed that by increasing the friction coefficient, the lateral resistance of the ballast was also increased. Finally, for the case of the sleeper with a greater displacement, a graph was obtained with a curve that resembles the curves obtained in the laboratory.

However, the analysis has some limitations, and obviously, the values obtained do not correspond to reality. This is due to the fact that the simulations are two-dimensional, so the bodies are considered as prisms and the two faces in the z direction are not taken into account.

For the study of the settlement of the sleeper, various cases have been studied, in which the number of elastic elements have been changed.

Through numerous simulations, graphs have been provided and they demonstrate how the stones move at certain points of the ballast after a load applied to the sleeper.

Automatically, graphs that show how the field of accelerations and speeds varies from the point most loaded to the less loaded point are plotted.

The software also allowed to demonstrate that there is an oscillatory behaviour due to the presence of elastic elements. Regarding the settlement of the sleeper, graphs that are similar to those seen in the literature are obtained.

The models seem therefore valid, albeit with values far from reality, but the results are very consistent.

Perspectives

After all the results explained in the previous sections, it is possible to say that the discrete element method and LMGC90 are reliable for the studies of the lateral resistance and the vertical settlement.

For the former, it is recommended to improve the compaction of the different zones of the ballast, trying to have a distribution very similar to the ballast after the tamping process. This is possible trying to create a high number of simulations.

For the latter, a simulation that lasts 300 seconds could not be enough. Future researchers could try to increase the time of the simulation, changing the friction coefficient and the compaction of the ballast. After that, it could be possible to correlate the results with the graph of the settlements, where the behaviour should be more or less the same. Furthermore, frequency response diagrams were also studied and it will be interesting to study the accelerations by a force with a constant frequency approaching the frequency peaks mentioned before.

The reader should not forget that all the simulations were carried out through 2D models, that doesn't represent perfectly the reality. 3D models are possible but they require a large amount of memory space as well as a large amount of time. If it took two days to analyse the settlement of a sleeper in 2D, in 3D it would take an entire week.

Bibliography

[1] Jacques Duran. *Sands, powders, and grains: an introduction to the physics of granular materials*. Springer Science & Business Media, 2012.

[2] Coenraad Esveld. Modern railway track, 2001.

[3] Infrabel. *Circulaire sur les traverses en béton M41*.

[4] Infrabel. *Spécification technique: fabrication et fourniture des traverses en béton monoblocs*.

[5] Infrabel. *Specification technique: fourniture de tapis amortisseurs sous ballast*.

[6] Sarah Knapton. Heatwave could buckle train tracks and melt roads, travellers warned.

[7] KTH Royal Institute of Technology. Rail vehicle dynamics.

[8] Vincent Legat. Méthodes numériques, 2011.

[9] Bernhard Lichtberger. Track compendium, 2005.

[10] Bernhard Lichtberger. Railway manual, 2010.

[11] LMGC90. LMGC90 documentation.

[12] Manuel Melis Maynar. *Apuntes de introducción a la dinámica vertical de la vía ya las señales digitales en ferrocarriles: con 151 programas en Matlab, Simulink, Visual C++, Visual Basic y Excel*. 2008.

[13] Official Journal of the European Union. Directive 2004/50/EC of the European Parliament and of the Council, April 2004.

[14] Chiara Paderno. Comportement du ballast sous l'action du bourrage et du trafic ferroviaire, 2010.

[15] Vassilios A Profillidis. Railway engineering, 2000.

[16] Juan-Carlos Quezada. *Mécanismes de tassement du ballast et sa variabilité*. PhD thesis, Université Montpellier II-Sciences et Techniques du Languedoc, 2012.

[17] Raül Acosta Suñé. Analyse numérique de la stabilité des voies ferrées, 2017.

[18] RFI. *Specifica tecnica: pietrisco per massicciata ferroviaria.*

[19] Gilles Saussine, C Cholet, PE Gautier, Frédéric Dubois, Claude Bohatier, and Jean-Jacques Moreau. Modelling ballast behaviour under dynamic loading. Part 1: A 2D polygonal discrete element method approach. *Computer methods in applied mechanics and engineering*, 195(19-22):2841–2859, 2006.

[20] Ernest Theodore Selig and John M Waters. *Track geotechnology and substructure management.* Thomas Telford, 1994.

[21] Shaishav Shah. BRM Kershaw - Ballast regulator machine.

[22] CJ Summers. The idiots guide to highways maintenance. 2005.

[23] Rayl System. Rail profile.

[24] UIC. *Loading Guidelines - Code of practice for the loading and securing of goods on railway wagons.*

[25] J van't Zand and J Moraal. Ballast resistance under three dimensional loading, 1997.

Appendices

A Profiles of the ballast

First profile:

$$y > 0.58 \ \wedge \ 0.36^2 < (x - 1.50)^2 + (y - 0.32)^2 \ \vee \ y > -0.73x + 1.81 \tag{A.1}$$

Second profile:

$$y > 0.33x + 0.14 \ \wedge \ y > 0.56 \ \vee \ y > -0.67x + 1.69 \tag{A.2}$$

This profile is a simplification of the first and in theory, they should have almost equal values.

Third profile:

$$y > 0.56 \ \vee \ y > -0.67x + 1.69 \tag{A.3}$$

Fourth profile:

$$y > 0.56 \ \vee \ y > -0.67x + 1.63 \tag{A.4}$$

B Oscillations of a two mass spring system

Another aim of this thesis is to find a relationship between a theoretical model, calculable with simple dynamics equations, and a model that can be calculated using the LMGC90 software. For this reason, it is necessary to consider the model consisting of two masses: m_2, i.e. the mass of the sleeper, and m_1, the mass of the ballast. Two elastic components have been added to this model: k_1, or the equivalent elastic component of the elastic layer placed just above the platform, and k_2, the equivalent elastic component of the elastic layer placed just below the sleeper, as shown in figure 4.20.

A 2D model with only two degrees of freedom and his vertical displacements are studied, obtaining also the accelerations and the frequencies of the bodies.

With the following equations, taken from a course in the KTH Royal Institute of Technology, in Stockholm, the procedure for obtaining the frequency response functions is described. [7]

$$\begin{cases} m_2\ddot{x}_2 + c_2\dot{x}_2 + c_2\dot{x}_1 + k_2x_2 + k_2x_1 = 0 \\ m_1\ddot{x}_1 - c_2\dot{x}_2 + (c_1 + c_2)\dot{x}_1 + k_2x_2 + k_2x_1 = 0 \end{cases} \tag{B.1}$$

In a short form:

$$M\ddot{x} + C\dot{x} + Kx = F \tag{B.2}$$

The values of the eigenvectors and eigenvalues must be found because they give important information about the dynamic properties of a track. The solution is found starting from the homogeneous equation:

$$M\ddot{x} + C\dot{x} + Kx = 0 \tag{B.3}$$

The solution of this equation should be in the form:

$$x(t) = \gamma \cdot e^{\lambda t} \tag{B.4}$$

Where γ are the eigenvalues and λ are the eingevectors of the system. Substituting this into the equation (B.3):

$$\det(\lambda^2 M + \lambda C + k) = 0 \tag{B.5}$$

It is possible to obtain:

$$m_2 m_1 \lambda^4 + (m_2 c_1 + m_2 c_2 + m_1 c_2)\lambda^3 + (m_2 k_1 + m_2 k_2 + m_1 k_2 + c_1 c_2)\lambda^2 + (c_1 k_2 + c_2 k_1)\lambda + k_1 k_2 = 0 \tag{B.6}$$

In this case, the model is considered undamped:

$$c_1 = 0,\ c_2 = 0 \tag{B.7}$$

From which it is obtained:

$$\lambda^2_{1,\,2} = -\frac{1}{2}\left[\frac{k_1}{m_1} + \frac{k_2}{m_2} \cdot \left(1 + \frac{m_2}{m_1}\right) \pm \sqrt{\left[\frac{k_1}{m_1} + \frac{k_2}{m_2} \cdot \left(1 + \frac{m_2}{m_1}\right)\right]^2 - \frac{4k_1 k_2}{m_1 m_2}}\right] \tag{B.8}$$

The eigenvectors are important because they give information on the amplitude of displacements and on the phase shift between the oscillations of the different masses.

Through the eigenvectors and the eigenvalues, it is possible to obtain the frequency response function: the quantitative measure of the output spectrum of a system in response to a stimulus, and it is used to characterise the dynamics of the system. It is possible to compute, for example, the behaviour of the accelerations for various frequencies and, through the graph, the frequency peaks can be analysed.

The excitation in the system has the equation:

$$F(t) = \bar{F} \cdot e^{\bar{s}t} \tag{B.9}$$

Consequently, the system respects with an equation like:

$$x(t) = \bar{x} \cdot e^{\bar{s}t} \tag{B.10}$$

By replacing this in (B.3):

$$(M\bar{s}^2 + C\bar{s} + K)\bar{x} = \bar{F} \tag{B.11}$$

It was decided to study the frequency response between force and acceleration, which has the form:

$$H_{\bar{F}_k}^{\ddot{x}_j}(\bar{s}) = \frac{\bar{s}^2 \cdot \bar{x}_j}{\bar{F}_k} = \bar{s}^2 \cdot H_{F_k}^{x_j}(\bar{s}) \tag{B.12}$$

Where:

- $\ddot{x}_j$ is the acceleration;
- $\bar{F}_k$ is the input;
- $\bar{s} = i\bar{\omega}$ is the frequency of the acceleration;
- $\bar{x}_j$ is the output;

With:

$$\begin{pmatrix} z_2 \\ z_1 \end{pmatrix} = \begin{pmatrix} \bar{z}_2 \\ \bar{z}_1 \end{pmatrix} e^{\bar{s}t} \tag{B.13}$$

equation (B.1) becomes:

$$\begin{vmatrix} m_2\bar{s}^2 + c_2\bar{s} + k_2 & -c_2\bar{s} - k_2 \\ -c_2\bar{s} - k_2 & m_1\bar{s}^2 + (c_1 + c_2)\bar{s} + (k_1 + k_2) \end{vmatrix} \tag{B.14}$$

The frequency response function between the applied force F and z_2 is written in the form:

$$H_F^{z_2}(\bar{s}) = \frac{\bar{z}_2}{F} \tag{B.15}$$

Remembering Cramer's rule:

$$\begin{bmatrix} a_1 & b_1 \\ a_2 & b_2 \end{bmatrix} \cdot \begin{pmatrix} x \\ y \end{pmatrix} = \begin{pmatrix} c_1 \\ c_2 \end{pmatrix} \tag{B.16}$$

the solutions are:

$$x = \frac{\det \begin{vmatrix} c_1 & b_1 \\ c_2 & b_2 \end{vmatrix}}{\det \begin{vmatrix} a_1 & b_1 \\ a_2 & b_2 \end{vmatrix}} \quad y = \frac{\det \begin{vmatrix} a_1 & c_1 \\ a_2 & c_2 \end{vmatrix}}{\det \begin{vmatrix} a_1 & b_1 \\ a_2 & b_2 \end{vmatrix}} \tag{B.17}$$

It is possible to obtain:

$$H_F^{z_2}(\bar{s}) = \frac{m_1\bar{s}^2 + (c_1 + c_2)\bar{s} + (k_1 + k_2)}{m_2m_1\bar{s}^4 + (m_2c_1 + m_2c_2 + m_1c_2)\bar{s}^3 + (m_2k_1 + m_2k_2 + m_1k_2 + c_1c_2)\bar{s}^2 + (c_1k_2 + c_2k_1)\bar{s} + k_1k_2} \tag{B.18}$$

The frequency response function between F and the acceleration of the second body is:

$$H_F^{\ddot{z}_2} = \frac{\bar{s}^2 \cdot \bar{z_2}}{F} = \bar{s}^2 \cdot H_F^{z_2}(\bar{s}) \tag{B.19}$$

It could be done the same with the first body:

$$H_F^{z_1}(\bar{s}) = \frac{z_1}{F} = \frac{\det \begin{vmatrix} m_2\bar{s}^2 + c_2\bar{s} + k_2 & 1 \\ -c_2\bar{s} - k_2 & 0 \end{vmatrix}}{\det \begin{vmatrix} m_2\bar{s}^2 + c_2\bar{s} + k_2 & -c_2\bar{s} - k_2 \\ -c_2\bar{s} - k_2 & m_1\bar{s}^2 + (c_1 + c_2)\bar{s} + (k_1 + k_2) \end{vmatrix}} \tag{B.20}$$

$$H_F^{z_1}(\bar{s}) = \frac{c_2\bar{s} + k_2}{m_2m_1\bar{s}^4 + (m_2c_1 + m_2c_2 + m_1c_2)\bar{s}^3 + (m_2k_1 + m_2k_2 + m_1k_2 + c_1c_2)\bar{s}^2 + (c_1k_2 + c_2k_1)\bar{s} + k_1k_2} \tag{B.21}$$

The frequency response function between the imposed force and the first body is given by:

$$H_F^{\ddot{z}_1} = \frac{\bar{s}^2 \cdot \bar{z_1}}{F} = \bar{s}^2 \cdot H_F^{z_1}(\bar{s}) \tag{B.22}$$

A system with two degrees of freedom has two frequency peaks, as shown in figure 4.21.

C Paraview

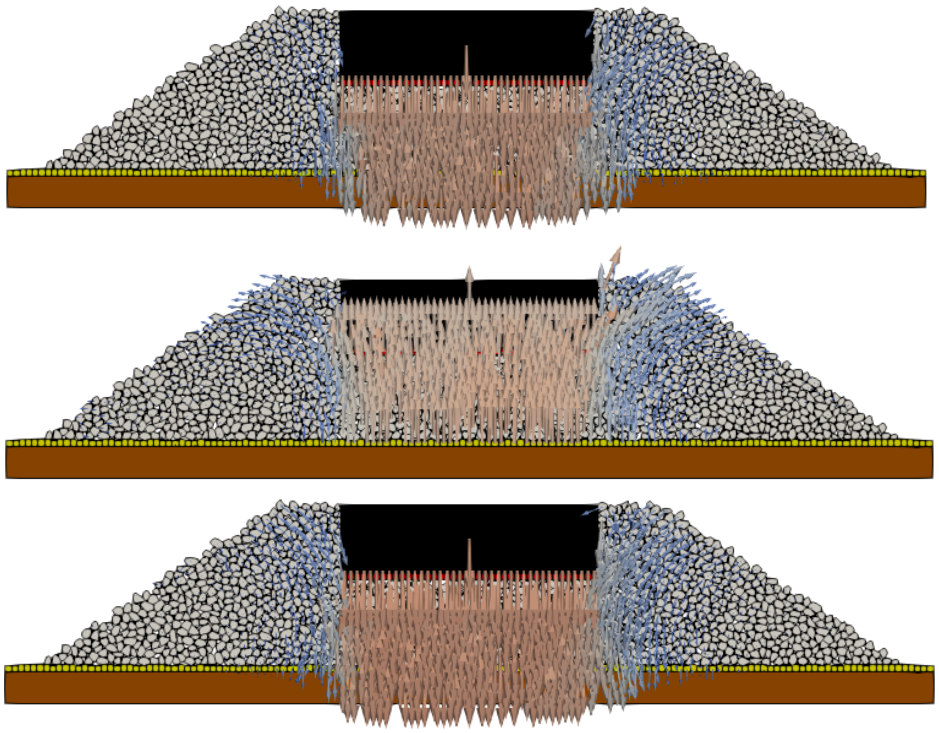

Figure C.1 – Velocity of the stones, respectively at $t = 1.000\ s,\ 1.025\ s,\ 1.100\ s$

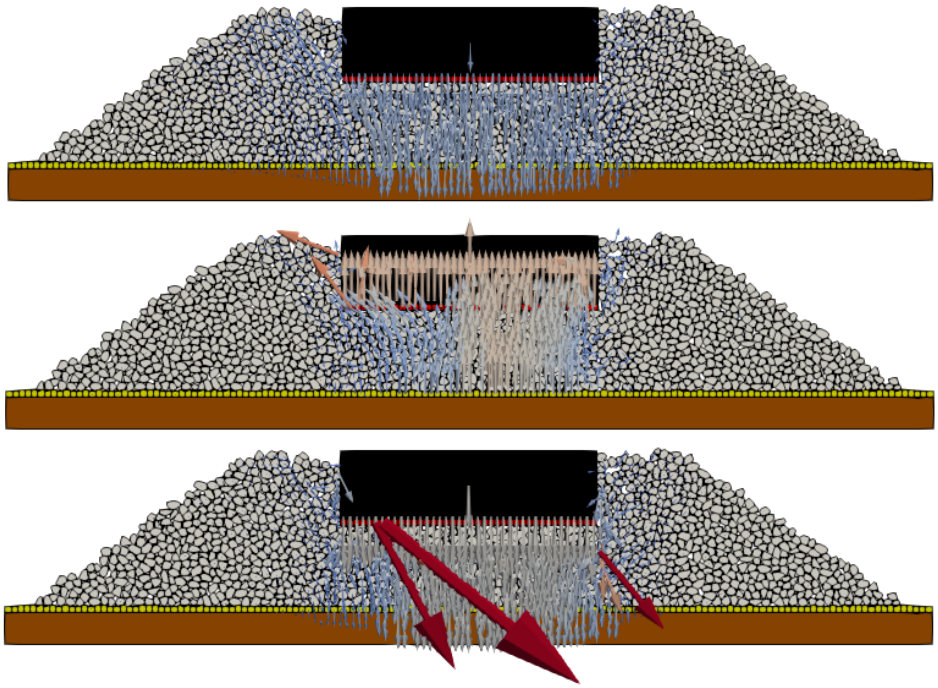

Figure C.2 – Velocity of the stones, respectively at $t = 100.000\ s,\ 100.025\ s,\ 100.100\ s$

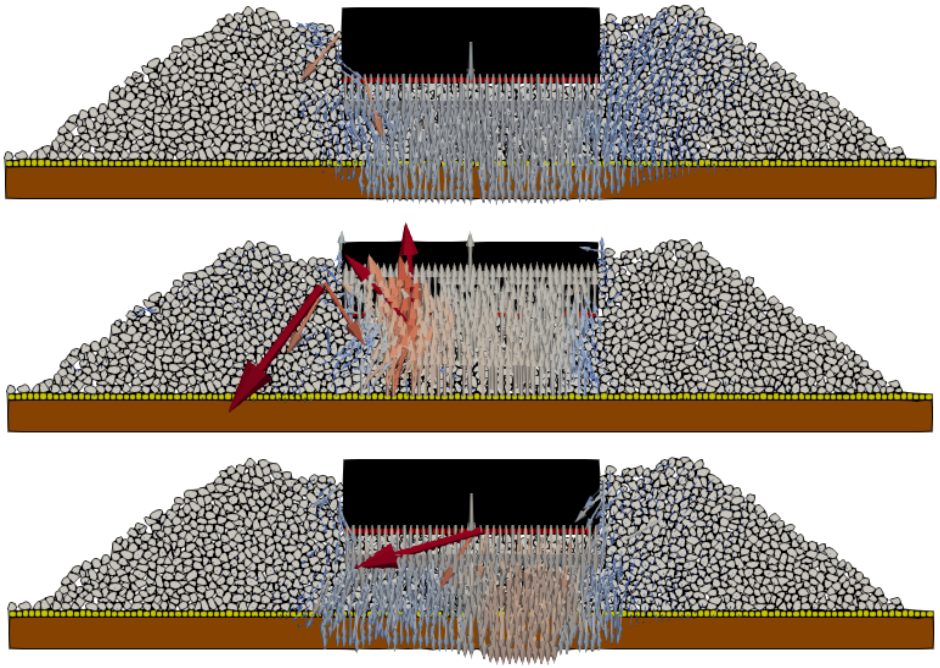

Figure C.3 – Velocity of the stones, respectively at $t = 199.000\ s,\ 199.925\ s,\ 200.000\ s$

Rue Archimède, 1 bte L6.11.01, 1348 Louvain-la-Neuve **www.uclouvain.be/epl**